PNNL-16509

Pacific Northwest
National Laboratory
Operated by Battelle for the
U.S. Department of Energy

Geostatistical Analyses of the Persistence and Inventory of Carbon Tetrachloride in the 200 West Area of the Hanford Site

C. J. Murray
Y.-J. Bott
M. J. Truex

April 2007

Prepared for Fluor Hanford, Inc.
under Contract DE-AC05-76RL01830
with the U.S. Department of Energy

DISCLAIMER

PACIFIC NORTHWEST NATIONAL LABORATORY
operated by
BATTELLE
for the
UNITED STATES DEPARTMENT OF ENERGY
under Contract DE-AC05-76RL01830

Printed in the United States of America

Available to DOE and DOE contractors from the
Office of Scientific and Technical Information,
P.O. Box 62, Oak Ridge, TN 37831-0062;
ph: (865) 576-8401
fax: (865) 576-5728
email: reports@adonis.osti.gov

Available to the public from the National Technical Information Service,
U.S. Department of Commerce, 5285 Port Royal Rd., Springfield, VA 22161
ph: (800) 553-6847
fax: (703) 605-6900
email: orders@ntis.fedworld.gov
online ordering: http://www.ntis.gov/ordering.htm


This document was printed on recycled paper.
(9/2003)

PNNL-16509

Geostatistical Analyses of the Persistence and Inventory of Carbon Tetrachloride in the 200 West Area of the Hanford Site

C. J. Murray
Y.-J. Bott
M. J. Truex

April 2007

Prepared for
Fluor Hanford, Inc.
under Contract DE-AC05-76RL01830
with the U.S. Department of Energy

Pacific Northwest National Laboratory
Richland, Washington 99352

Preface

Background

The U.S. Department of Energy Hanford Site was the main plutonium production facility for the American nuclear weapons program between 1944 and 1988. Waste disposal from chemical processing in the 200 West Area in the central part of the Site resulted in the discharge of large quantities of contaminated water to the subsurface. Contaminants included radionuclides, metals, nitrate, and volatile organic compounds.

One of the most widespread and significant contaminants in the 200 West Area is carbon tetrachloride (CT). Carbon tetrachloride was used in the final plutonium purification process at the Plutonium Finishing Plant, which was constructed in 1949 in the 200 West Area. Three nearby disposal facilities received 570,000 to 920,000 kg of spent CT (as both dissolved and separate liquid phases) between 1955 and 1973.

Limited groundwater monitoring for radionuclides in the 200 West Area began by 1948, making this one of the oldest groundwater contaminant monitoring programs in the world. Analysis of volatile organic compounds by the monitoring program began in 1987 and defined the CT plume at the top of the aquifer. As of 1999, the plume was found at levels above the 5-μg/L drinking water standard over approximately 11.5 km^2 of the Site.

Previous work on the CT plume in the Hanford Site 200 West Area indicates that 65% of approximately 750,000 kg of CT that was delivered to the ground as a result of plutonium processing remains unaccounted for. In addition, the results of groundwater monitoring have been used to suggest that persistent sources of CT may be feeding the contaminant plume in the aquifer.

Report Scope

This report documents two separate geostatistical studies performed by researchers from Pacific Northwest National Laboratory (PNNL) to evaluate the CT plume in the groundwater.

The first chapter of the report examines and evaluates a number of potential continuing source locations within the unconfined aquifer that had been identified in the 200 West Area by Fluor Hanford, Inc. (FH), based on locally elevated carbon tetrachloride groundwater concentrations. FH requested that PNNL perform a geostatistical study of the persistence of CT groundwater concentration values over time in those areas. This work was completed in 2005, and a letter report describing the work was sent to FH. The first chapter of this report is a reformatted version of that letter report, with no update of the analysis.

The second chapter of this report followed from a request by FH that PNNL re-evaluate the inventory of CT in the unconfined aquifer in the 200 West Area and perform a 3D geostatistical study of the deep CT groundwater concentration values available in the area. An initial study was completed as a letter report to FH in January 2006, based on depth-discrete data collected during the drilling process. The second chapter of this report documents an updated version of that study, incorporating additional data available through November 2006 and also incorporating 3D concentration data from existing wells collected using packers to attempt to isolate and sample restricted depth intervals in the wells.

Contents

Figures

Tables

Chapter 1

Geostatistical Analysis of the Persistence of Carbon Tetrachloride Groundwater Concentrations in the 200 West Area of the Hanford Site[(a)]

Christopher J. Murray and Yi-Ju Bott

Summary

Data sets of average annual carbon tetrachloride (CT) concentrations were developed for four time periods—1996, 1998, 2000, and 2002. These data sets had consistent locations for each time period so that variations in concentration with time in a given area would be due to changes in concentrations and not to just changes in the configuration of data locations. A fifth data set was added to represent conditions in 2004. Although the results for the 2004 time period generally agreed with results for the earlier time periods, the change in data locations makes the results for that last time period more uncertain. No significant differences were seen in the overall distribution of CT concentrations over the 10-year time period studied, although there was an indication of a slight decrease in concentrations during the last two time periods.

The CT concentration data were highly skewed, so concentration mapping was performed on normal score transforms of the data. Experimental variograms were fit with isotropic models that showed a slight decrease in range from 1200 m in 1996 and 1998 to 1000 m in 2000 and 2002. The variogram range in 2004 was even shorter, but that may be an artifact of change in data locations for the last time period, although the decrease in range might also be due to a slight decrease in the size of the plume with time.

We generated 1000 simulations of CT concentration for each time period and found that 500 simulations were sufficient to characterize the spatial variability in CT concentration. The spatial distribution of CT was summarized in several ways, including calculation of median simulated values, the probability of exceeding several cutoff values, and calculation of percentiles of the local distributions. Maps prepared from those statistics identified areas of high and low concentration for each time period and provided measures of the uncertainty in concentration. These were used to rank sub-areas identified by Fluor Hanford, Inc. (FH) in terms of their likelihood of containing persistent CT sources.

Introduction

Previous work on the CT plume in the 200 West Area of the Hanford Site indicates that a large amount of the CT delivered to the ground as a result of plutonium processing remains unaccounted for. In addition, there have been suggestions that the missing CT provides continuing sources of contamination that affect the unconfined aquifer beneath the Site.

(a) Chapter 1 was prepared originally as a letter report and issued to Fluor Hanford, Inc. on August 3, 2005.

To examine and evaluate a number of potential continuing source locations identified in the 200 West Area, FH requested that PNNL perform a geostatistical study of the persistence of CT groundwater concentration values over time. This chapter documents the results of that study.

Methods

Because the main focus was on identifying the persistence of areas with high groundwater CT concentrations over time, it was important to attempt to find a set of locations sampled consistently in all periods. Previous geostatistical analysis by the authors (e.g., Peterson et al. 2005) had found that contaminant plume maps were somewhat sensitive to changes in the distribution of monitoring well locations over time. An analysis was performed of the available CT data for the period from 1994 to 2004 using annual averages of CT concentrations. Only CT data meeting the standard laboratory and review qualifier criteria employed by the PNNL Groundwater Performance Assessment Project were included in the annual averages. Initially, four data sets were selected, with 53 locations for which CT data were consistently available for 1996, 1998, 2000, and 2002 (Figure 1.1). Those locations appeared to provide reasonable control on the concentration distribution for each of the eight areas of interest selected by FH and are shown in Figure 1.1.

After initial review of the results for the 1996-2002 CT data, we were requested to add a fifth data set to represent the 2004 time period. Only 37 of the 53 locations used for the 1996-2002 time periods had data available from 2004 (Figure 1.2). An additional 11 wells included in the 1996-2002 analysis had data available from 2003, so those were included with the 2004 data set. The combined 2003-2004 data set has 48 locations identical to those used for 1996-2002 (Figure 1.2).

The concentration data from each time period were plotted and summarized. The geostatistical method used for the study was sequential Gaussian simulation (Goovaerts 1997). That method is based on use of a normal score transform of the data that transforms the data so that they are normally distributed with a mean of zero and a variance of 1. This transform, similar in its effect to a logarithmic transform, adjusts for the positively skewed nature of the CT concentrations but has several advantages for geostatistical modeling over a logarithmic transform. Variograms of the normally transformed data were calculated and used to estimate a model for the spatial continuity of the data. The variogram models were used in turn as input to the sequential Gaussian simulation program, SGSIM (Deutsch and Journel 1998). A suite of 1000 simulations of the CT concentration was generated for each time period using a rectangular grid with spacing of 50 m in the easting and northing directions. Each simulation honors the available data and the variogram model and is an equally likely map of the CT concentrations. Several algorithms then were used to summarize and map the simulation results. These included calculation of the median simulated value at each node of the simulation grid, the 10th percentile of the simulated concentration values, and the probability of exceeding several concentration thresholds, including 5 µg/L (the drinking water standard or DWS), 100 µg/L, 500 µg/L, 1000 µg/L, and 2000 µg/L. The results for each of the eight areas of interest identified by FH personnel were extracted from the maps and presented graphically. Box plots also were used to compare the areas for a given point in time and to compare the results for the same area for the different time periods.

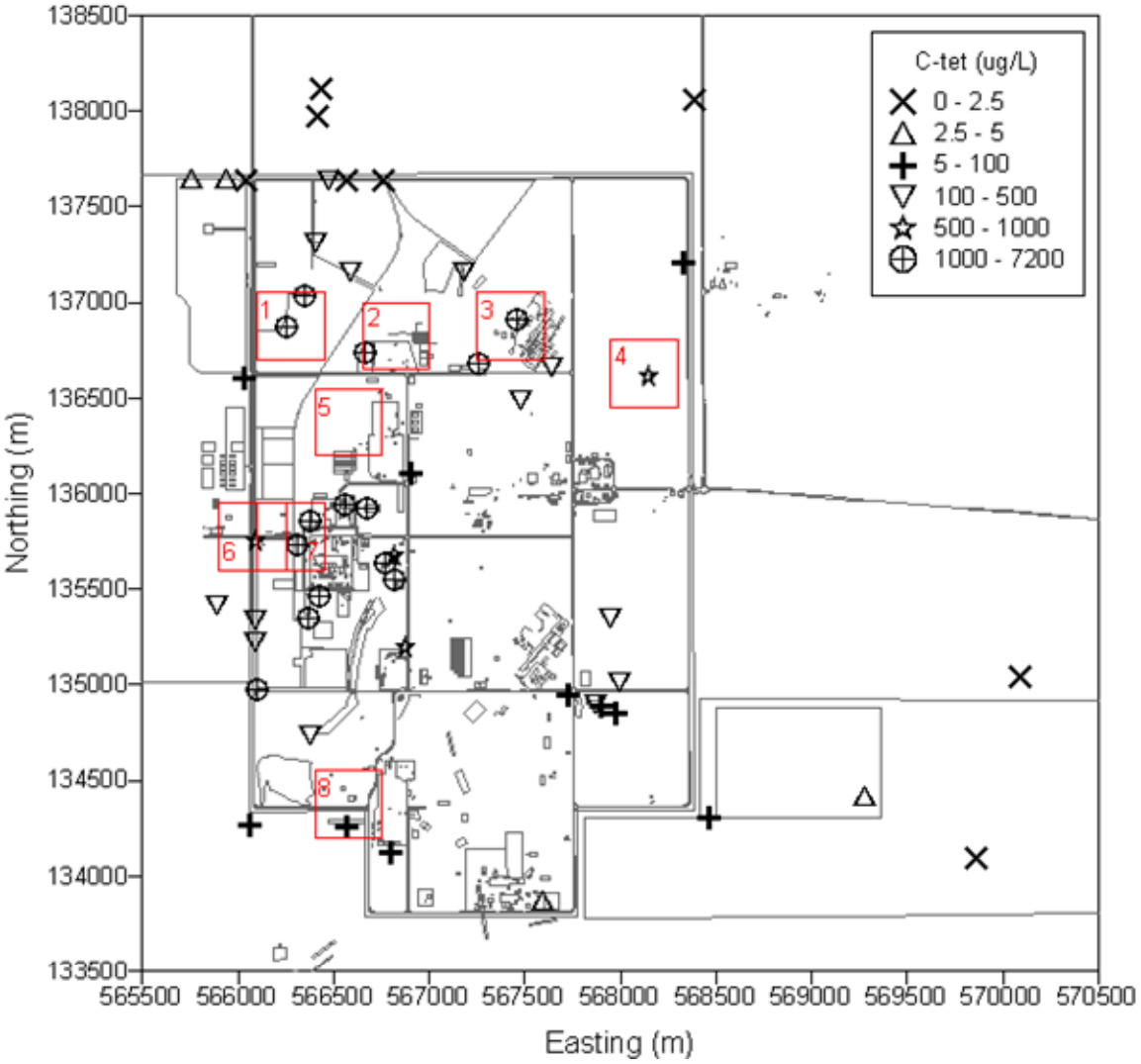

Figure 1.1. Locations of 53 Wells Used To Map CT Data for Four Time Periods (1996, 1998, 2000, 2002). Eight areas of interest are highlighted in red.

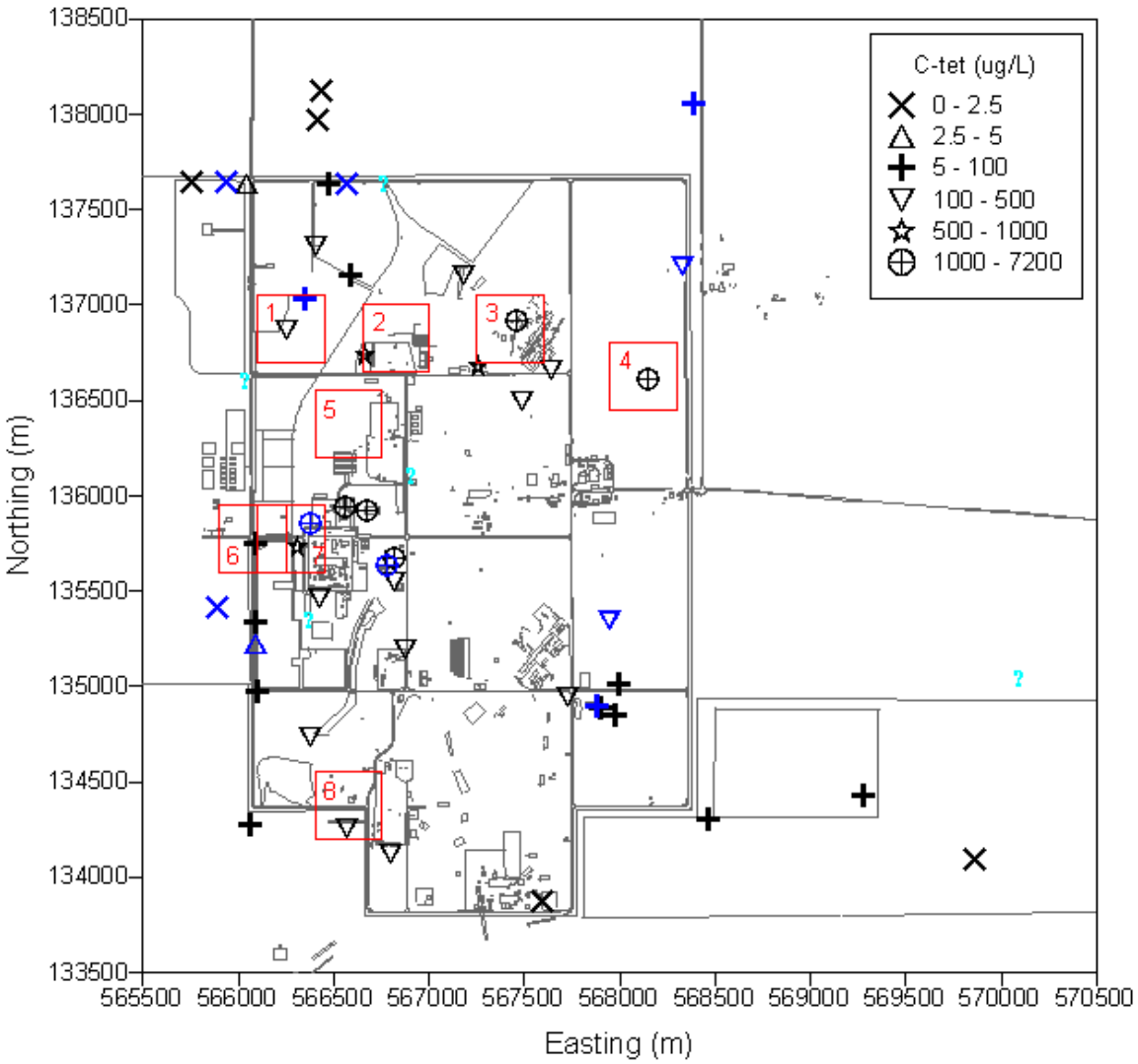

Figure 1.2. Locations of 37 Wells (of those shown in Figure 1.1) with Data Available for 2004 (in Black), 11 Wells with 2003 Data (in Blue), and Five Wells Without Measurements (in Light Blue)

Results

Figure 1.3 shows the distribution of CT data for each time period, with a tabular summary in Table 1.1. The box plots are plotted on a logarithmic scale because the CT data are highly skewed. This can be seen in Table 1.1, where the mean values for each year are three to seven times higher than the median values. There appear to be slight decreases in both the mean and median CT values for the last two observation periods (2002 and 2004), but those decreases are not significant due to the high variability of the data. Both the notches around the median and the 95% confidence limits around the mean indicate substantial overlap between the CT data for all years.

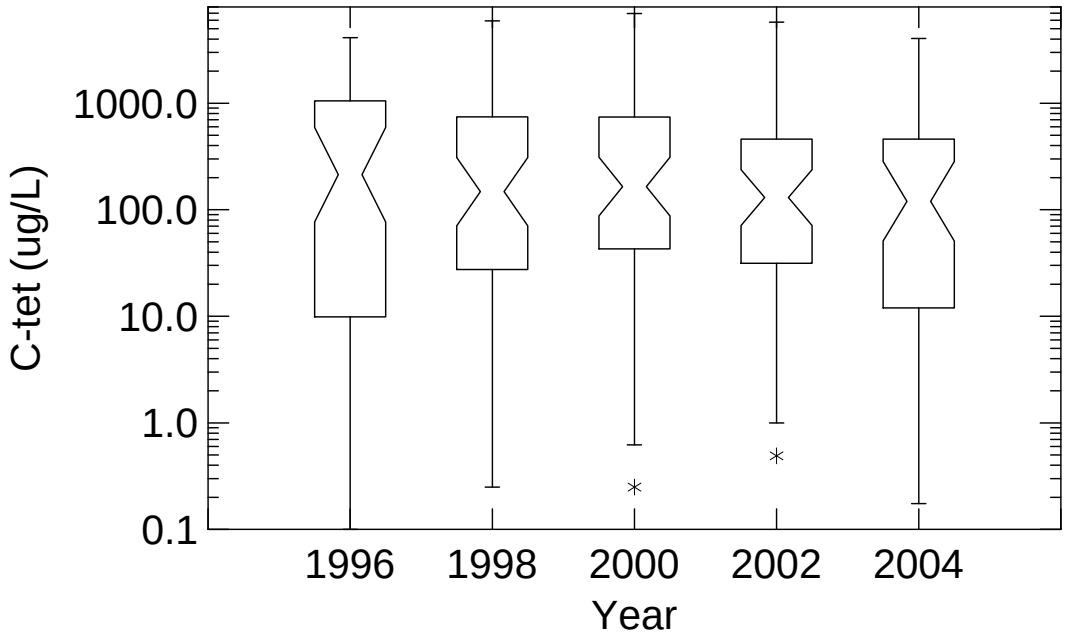

Figure 1.3. Distribution of CT Data for Each Time Period

Table 1.1. Summary Statistics of CT Concentration for Each Time Period

CT (µg/L)	1996	1998	2000	2002	2004
Mean	621.827	763.727	782.180	552.765	445.791
Standard Error	124.537	201.496	213.357	162.108	121.503
Median	193.333	115.667	140.000	94.000	99.417
Standard Deviation	906.640	1466.910	1553.261	1180.164	841.796
Kurtosis	5.043	5.998	7.186	10.222	7.712
Skewness	2.165	2.592	2.741	3.151	2.706
Range	4123.333	5917.750	6933.333	5750.000	4040.500
Minimum	0	0	0	0	0
Maximum	4123.333	5917.750	6933.333	5750.000	4040.500
Count	53	53	53	53	48
Confidence Level of Mean (95.0%)	249.901	404.330	428.132	325.293	244.432

Because the data are highly skewed, we performed the geostatistical analysis on a normal score transform (Deutsch and Journel 1998). The normal score transform is an alternative to a logarithmic transformation that has several advantages over that transformation. We calculated the experimental variogram of the normal score transformed CT data for each time period (Figure 1.4) and fit the variogram using spherical variogram models (Deutsch and Journel 1998). As in previous 2D studies of CT concentration data from the 200 West Area, no directional anisotropy was detected; i.e., the spatial continuity appeared to be approximately equal in all directions, so the variogram models for each year were isotropic models. The range of continuity of the variogram decreased slightly, from 1200 m in 1996 and 1998 to 1000 m in 2000 and 2002, with a possible further decrease to 500 m in 2004 (keeping in mind that the range for the 2004 data may be influenced by the lack of data for five of the samples used for the earlier periods).

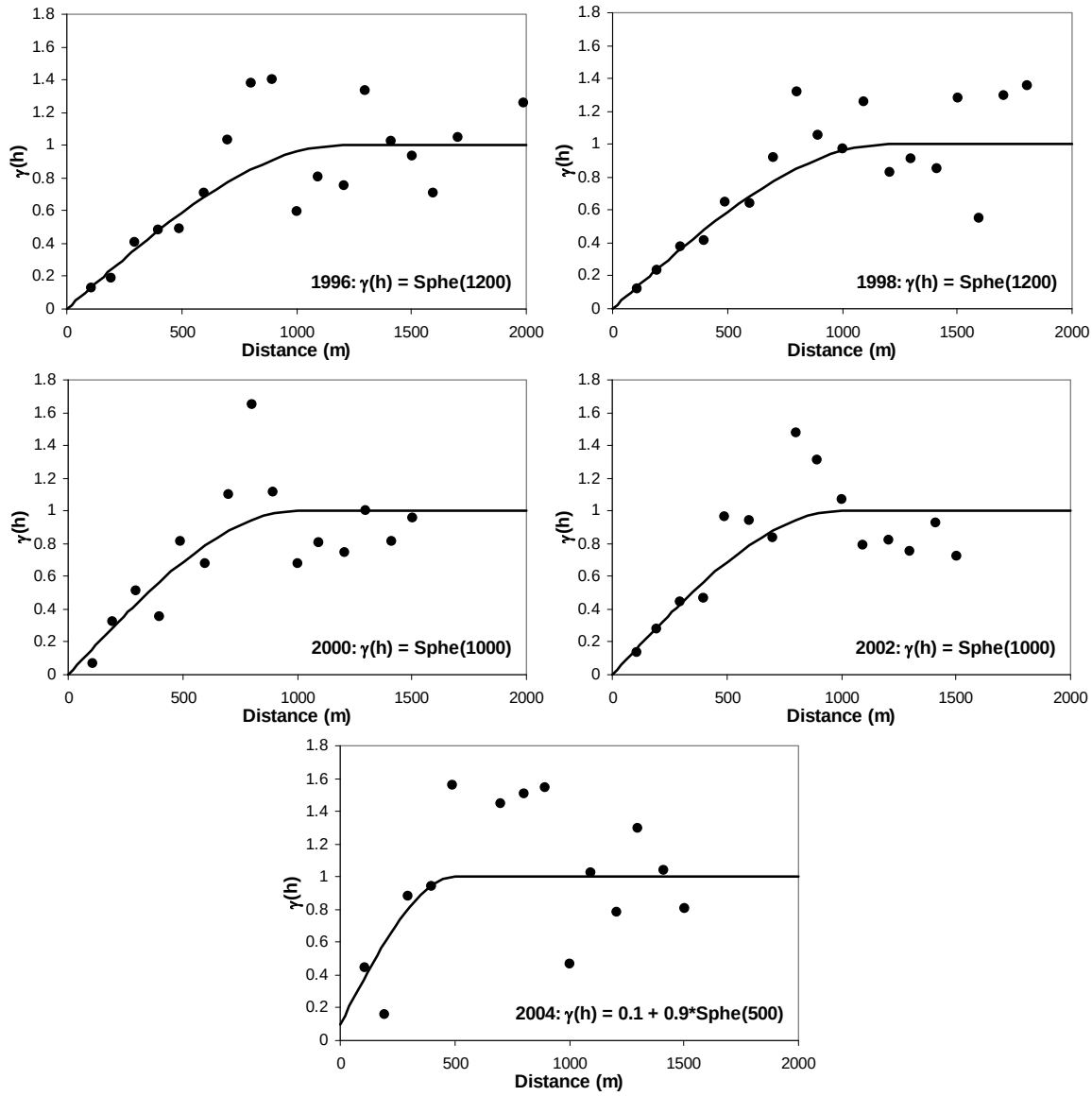

Figure 1.4. Omnidirectional Variograms and Models of Normal Scores of CT Data by Year

The variogram models and CT concentration for each time period were used as input to the sequential Gaussian simulation program, SGSIM (Deutsch and Journel 1998), and 1000 simulations of the CT concentration were generated for each time period. Examination of the mean and variance of the area above 2000 μg/L indicated that 500 simulations were sufficient to characterize the variability in CT concentration, so 500 simulations were used in the summary evaluations discussed below. The suites of simulations provide 500 simulated values of CT concentration at every grid node in the study area; these values can be used to estimate the probability distribution of the CT concentration at each grid node. These local probability distributions were summarized in several ways. One was to calculate the median simulated value at each grid node, which provides a robust measure of the center of the distribution. The median concentration maps for each time period are plotted in Figures 1.5 through 1.9. The map on the right-hand side of each figure contains the isolated median maps for each of the eight sub-areas of interest identified by FH personnel. Note that the northeast quarter of the map is very poorly constrained, with no data present in that area, but none of the sub-areas of interest falls in that area.

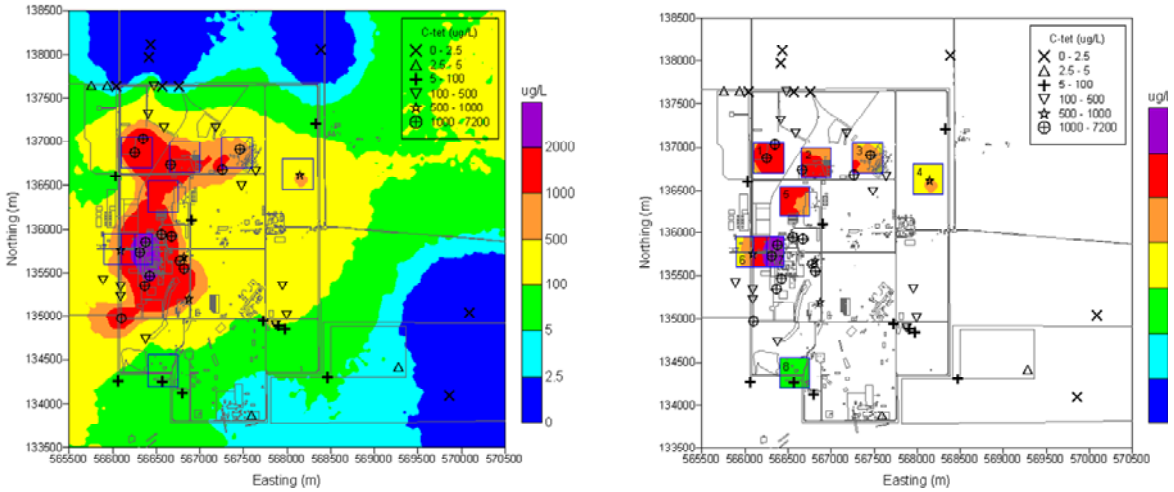

Figure 1.5. Medians of Simulated CT in 1996 with Eight Sub-Areas Isolated

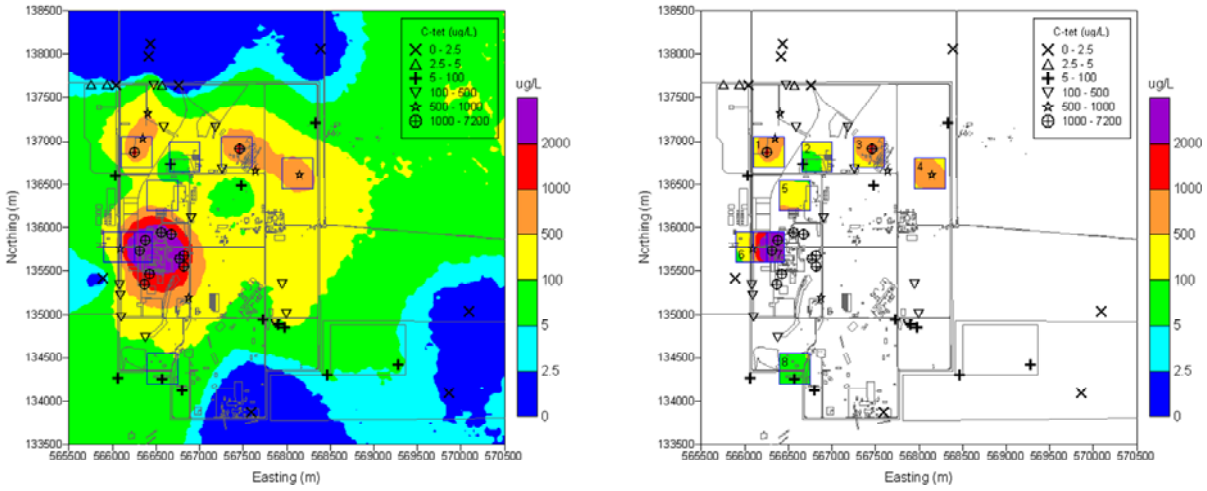

Figure 1.6. Medians of Simulated CT in 1998 with Eight Sub-Areas Isolated

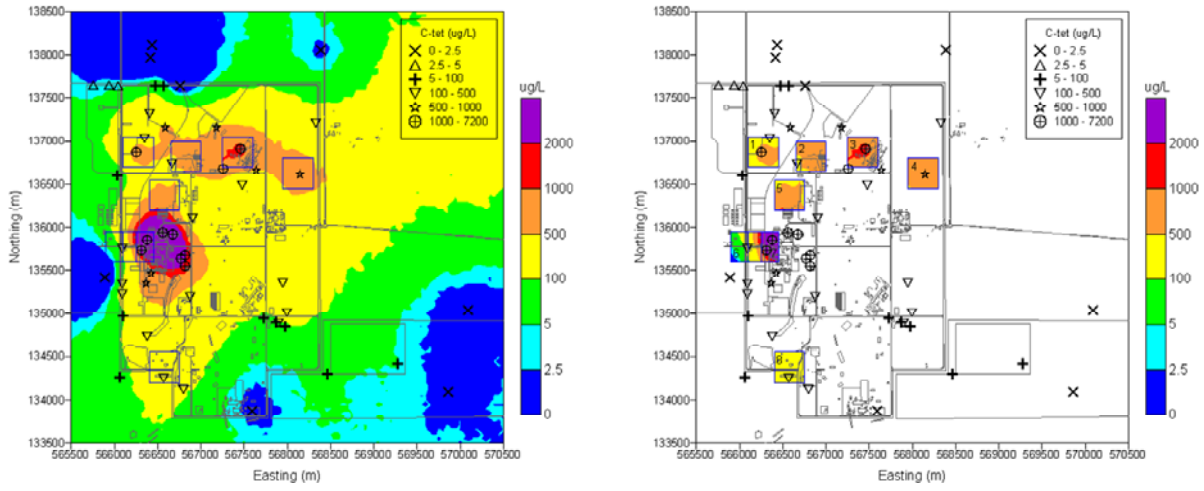

Figure 1.7. Medians of Simulated CT in 2000 with Eight Sub-Areas Isolated

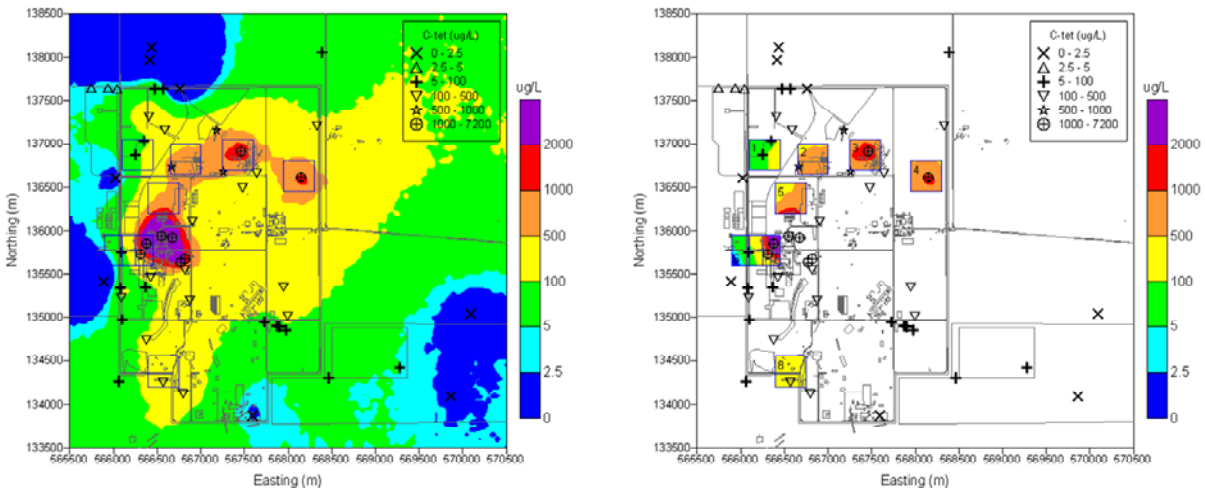

Figure 1.8. Medians of Simulated CT in 2002 with Eight Sub-Areas Isolated

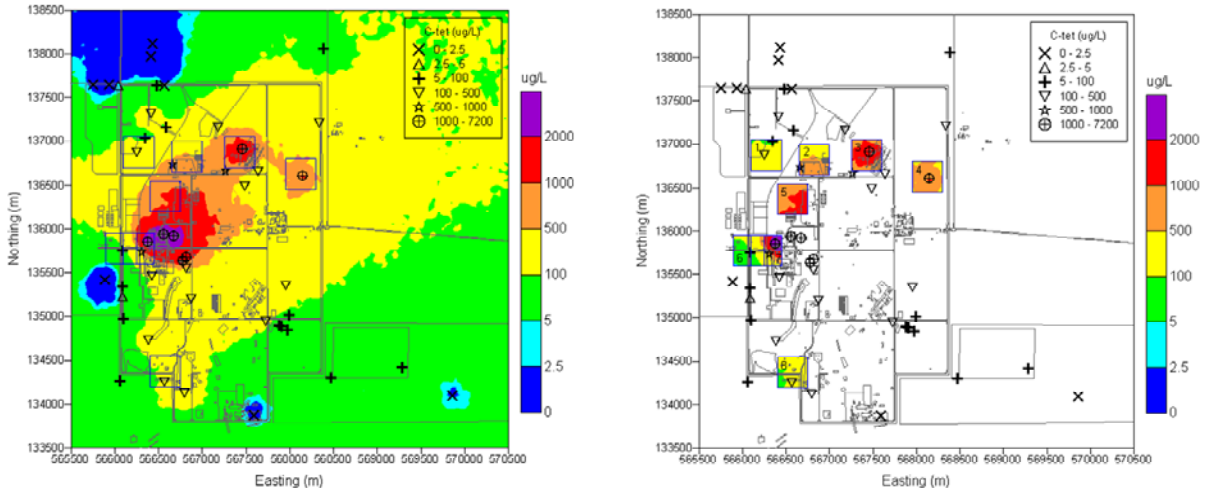

Figure 1.9. Medians of Simulated CT in 2004 with Eight Sub-Areas Isolated

Additional sets of summaries used to compare the eight sub-areas were the probability of exceeding several different concentration limits and the 10th percentiles of the simulated CT values. Figure 1.10 presents probability maps for several cutoffs, including 5 µg/L, 100 µg/L, 500 µg/L, 1000 µg/L, and 2000 µg/L for the 2002 time period. Figure 1.11 contains results for the 10th percentiles of the distributions at each grid node. Because 90% of the simulated CT values were higher than those plotted on the 10th percentile maps, areas shown with high concentrations on the maps shown in Figure 1.11 can be used to identify areas that almost certainly have a high concentration. The shapes of the 10th percentile maps are quite consistent in Figure 1.11, especially for the time periods from 1996 through 2002 when all the data locations were constant.

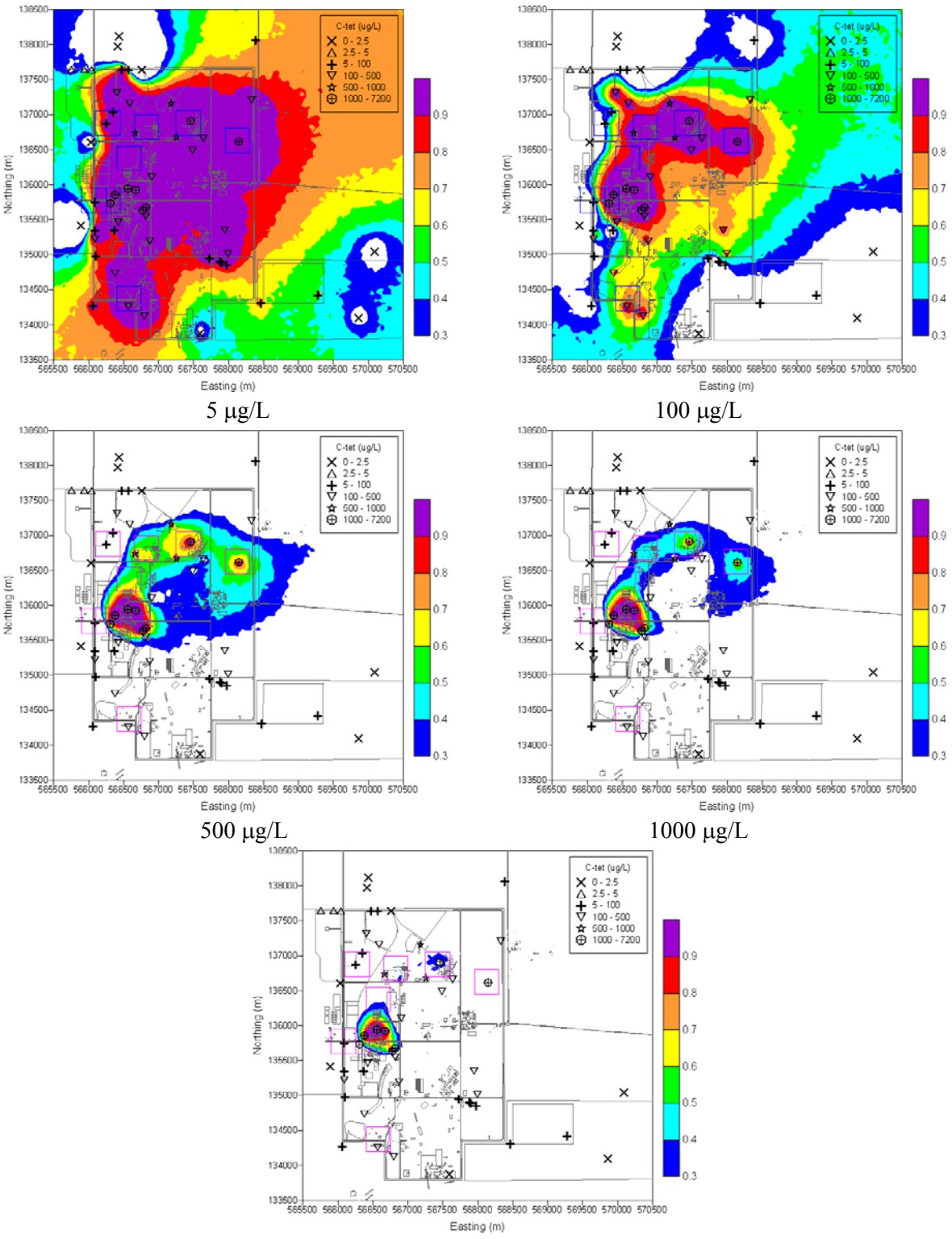

Figure 1.10. Probability of Exceeding Five Different CT Concentration Levels in 2002

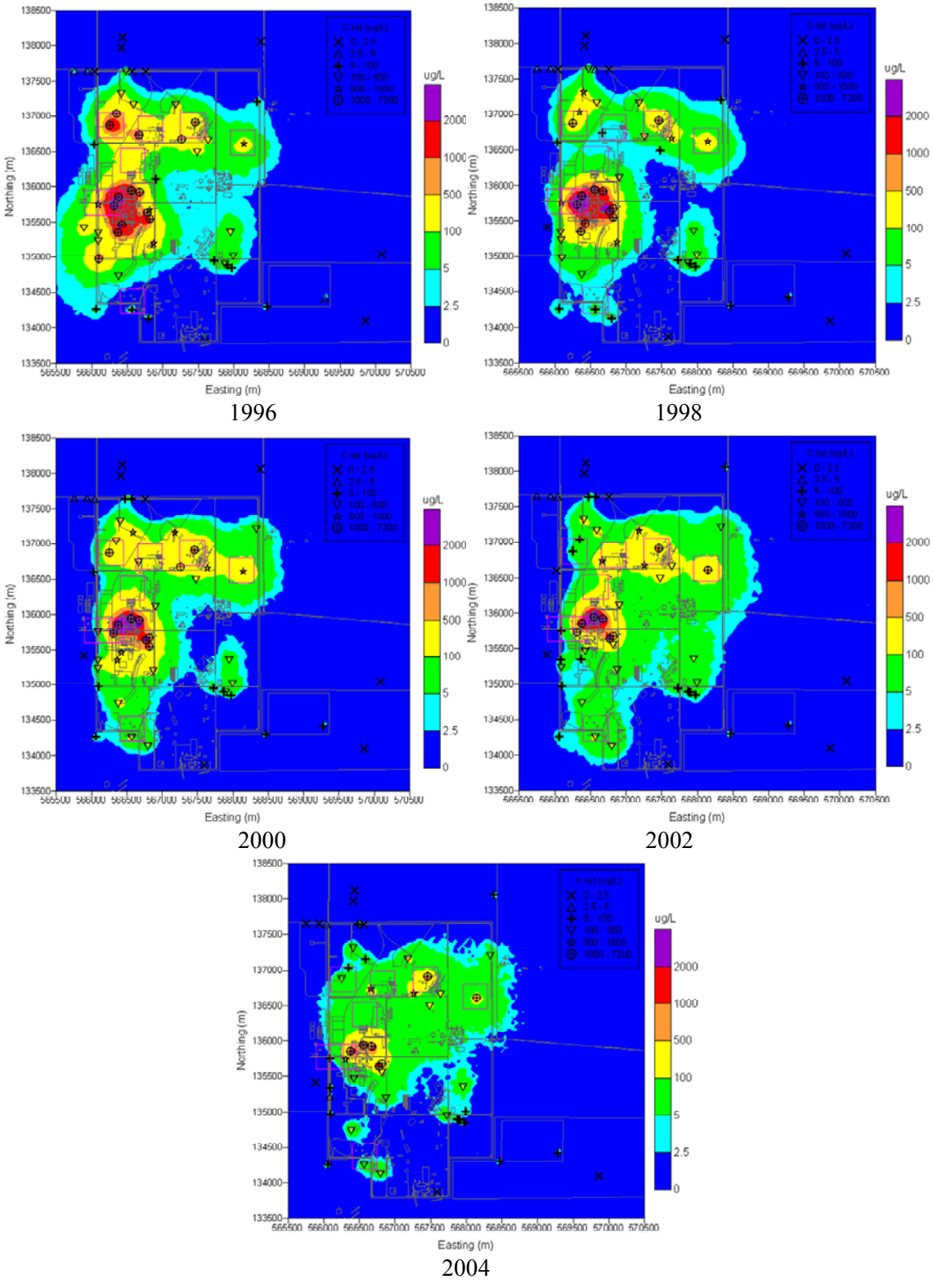

Figure 1.11. The 10th Percentiles of Simulated CT for 1996 Through 2004

A set of box plots (Figure 1.12) compares the median simulated CT values within each sub-area over the five time periods. The upper and lower margins of each box in the box plots represent the 75th and 25th percentiles of the data; the center of the notched area of the box represents the median; and the whiskers show the range of values that fall within 1.5 times the interquartile range of the hinge (where the interquartile range is 75th percentile–25th percentile). Values beyond the whiskers are identified as outliers. The notches around the median values represent a robust estimate of a 95% confidence interval around the median, so that boxes where the notches overlap are not significantly different from one another. Note that the CT concentrations plotted for all box plots are on a logarithmic scale. Several important results can be seen in Figure 1.12. First, several of the northern sub-areas, especially areas 2, 3, 4, and 5, have relatively high median values over time, with low variability around that median and a median relatively constant over time. This indicates that the simulated CT concentrations in those sub-areas tend to be relatively constant at higher concentration values. Sub-areas 1 and 6 show much larger fluctuations in CT concentration over time, with substantial decreases in CT concentration over time. Sub-area 7 also shows a significant decrease in median concentrations over time (and an increase in variability), but remains at relatively high levels even after that decrease (nearly 500 μg/L.) Sub-area 8 shows an increase over time (Figure 1.12) but still has the lowest median concentration levels of any of the sub-areas after that increase, remaining less than 200 μg/L.

The lower values seen for sub-areas 2 and 5 in 1998 (Figure 1.12) were strongly influenced by the groundwater concentrations for well 299-W10-1. The CT concentration reported for that location in 1998 was 38 μg/L, while the remainder of the CT concentrations reported for that well ranged from 450 to 1500 μg/L for the period from 1996 to 2004. The laboratory and review qualifiers for the 1998 concentration for well 299-W10-1 do not contain any indication that the results were considered suspect. However, if the low value for that well in 1998 was actually due to lab or sampling error and the concentration should have been closer to what was found in the other time periods, then sub-areas 2 and 5 might have had median simulated values for 1998 that would be similar to those seen for sub-areas 3 and 4 in Figure 1.12.

Table 1.2 contains the median simulated CT values from Figure 1.12 for each sub-area by year, which may make it easier to compare behavior of the concentrations in the sub-areas over time. Figure 1.13 contains box plots of the median simulated CT concentrations accumulated for each sub-area over all the time periods. As with Figure 1.12, it shows that the smallest variability in median CT concentration over time can be found in sub-areas 3 and 4, and that both of those areas also have relatively high concentrations. Sub-areas 2 and 5 show slightly greater variability with time but also have high concentrations and fairly low variability. The highest concentrations over time are found in sub-area 7, but that sub-area also has a relatively high variability over time.

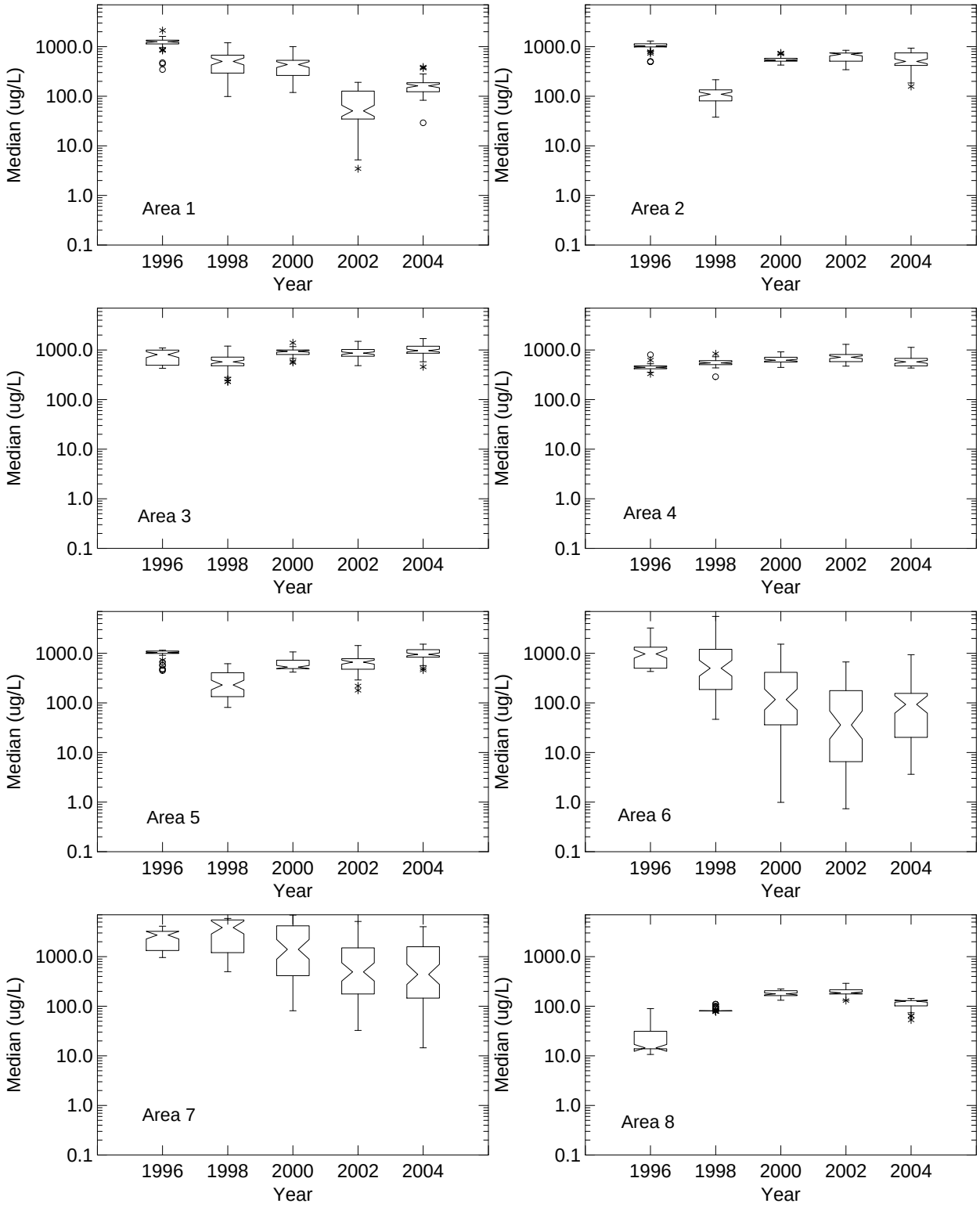

Figure 1.12. Medians of Simulated CT by Year for Sub-Areas 1 to 8

Table 1.2. Median Simulated CT of each Sub-Area by Year

1996		1998		2000		2002		2004	
Area	Median	Area	Median	Area	Median	Area	Median	Area	Median
7	2720.663	7	3878.445	7	1407.160	3	865.902	3	972.3904
1	1256.494	3	577.636	3	942.908	4	714.837	5	952.7022
5	1042.485	4	550.705	4	623.829	2	701.554	4	577.5723
2	1025.800	1	504.395	2	536.936	5	664.971	2	506.3968
6	972.554	6	500.975	5	527.903	7	493.452	7	439.8412
3	809.009	5	230.000	1	435.660	8	186.660	1	161.9432
4	447.936	2	110.000	8	177.888	1	50.915	8	126.8342
8	14.498	8	81.017	6	117.238	6	36.056	6	93.4274

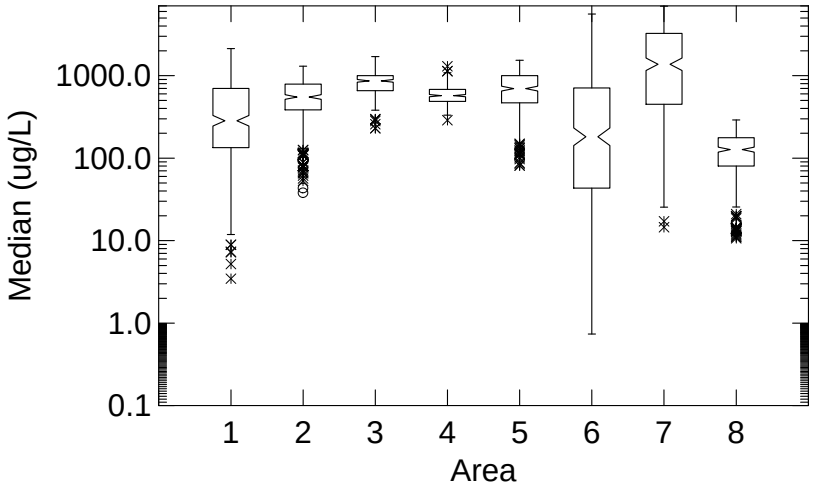

Figure 1.13. Median Simulated CT from 1996 to 2004 by Sub-Area

Discussion and Conclusions

Data sets of average annual CT concentration were developed for four time periods—1996, 1998, 2000, and 2002. These data sets had consistent locations for each time period so that variations in concentration with time in a given area would be due to changes in concentrations, and not just to changes in the configuration of data locations. A fifth data set was added to represent conditions in 2004 that included data from 37 locations for 2004 and from 11 locations for 2003. Data for five locations sampled in the other four years were not collected in 2004 or 2003. Although the results for the 2004 time period generally agreed with results for the earlier time periods, the change in data locations makes the results for that last time period more uncertain. No significant differences were seen in the overall distribution of CT concentrations over the 10-year time period that was studied, although there was an indication of a slight decrease in concentrations during the last two time periods.

The CT concentration data were highly skewed, so concentration mapping was performed on normal score transforms of the data. Experimental variograms were fit with isotropic models that showed a slight decrease in range from 1200 m in 1996 and 1998 to 1000 m in 2000 and 2002. The variogram range in 2004 was even shorter, but that may be an artifact of change in data locations for the last time period, although the decrease in range might also be due to a slight decrease in the size of the plume with time.

We generated 1000 simulations of CT concentration for each time period and found that 500 simulations were sufficient to characterize the spatial variability in CT concentration. The spatial distribution of CT was summarized in several ways, including calculation of median simulated values, the probability of exceeding several cutoff values, and calculation of percentiles of the local distributions. Maps prepared from those statistics identified areas of high and low concentration for each time period, and provided measures of the uncertainty in concentration.

The simulation results for the individual sub-areas of interest outlined by FH personnel identified important differences between the sub-areas. Those differences suggest that some of the sub-areas might contain ongoing CT sources. These results include the following:

- Several of the northern sub-areas had relatively high median concentrations with low variability, and little variation with time. This suggests that these would be sub-areas that might contain continuing sources. The sub-areas with the highest median concentrations and lowest variability were sub-areas 3 and 4. Sub-areas 5 and 2 would also be candidates, although they display greater variability over time. Recall that if the concentration reported for well 299-W10-1 for 1998 is not representative and should have been similar to those in other years, then the median concentrations of sub-areas 2 and 5 would be higher and they would show less variability, which would make them look very similar to sub-areas 3 and 4.
- Sub-area 7 shows a significant decrease in median concentration over the last two time periods, suggesting that concentrations in that area have substantially decreased, possibly due to the pump-and-treat remedial action taking place near that sub-area.
- Sub-areas 6 and 1 also show significant decreases in median concentration over time and seem unlikely to contain continuing CT sources. Sub-area 8 shows an increasing median CT concentration with time, but concentrations in that sub-area remain significantly lower than all of the other sub-areas, indicating that it is unlikely to contain a significant continuing source of CT.

Figure 1.14 is a summary map that shows the ranking of the sub-areas identified by FH personnel in terms of their likelihood of containing persistent CT sources. Note that these results should not be understood in terms of identifying the main source of the CT plume present in the 200 West Area, but of identifying areas where apparently persistent high local concentrations of CT in the groundwater may indicate the presence of continuing sources. As such, they suggest that undiscovered sources may exist in the vadose zone or aquifer in those areas, the nature and location of which would need to be verified by additional characterization.

Overall, the results suggest that the geostatistical approach developed for this study provides a good method of analyzing changes in the spatial distribution of CT with time, and then using that information to evaluate the potential for continuing local sources to be present in focus areas within the overall study area. Additional ground truth data will be needed to determine the accuracy of the method.

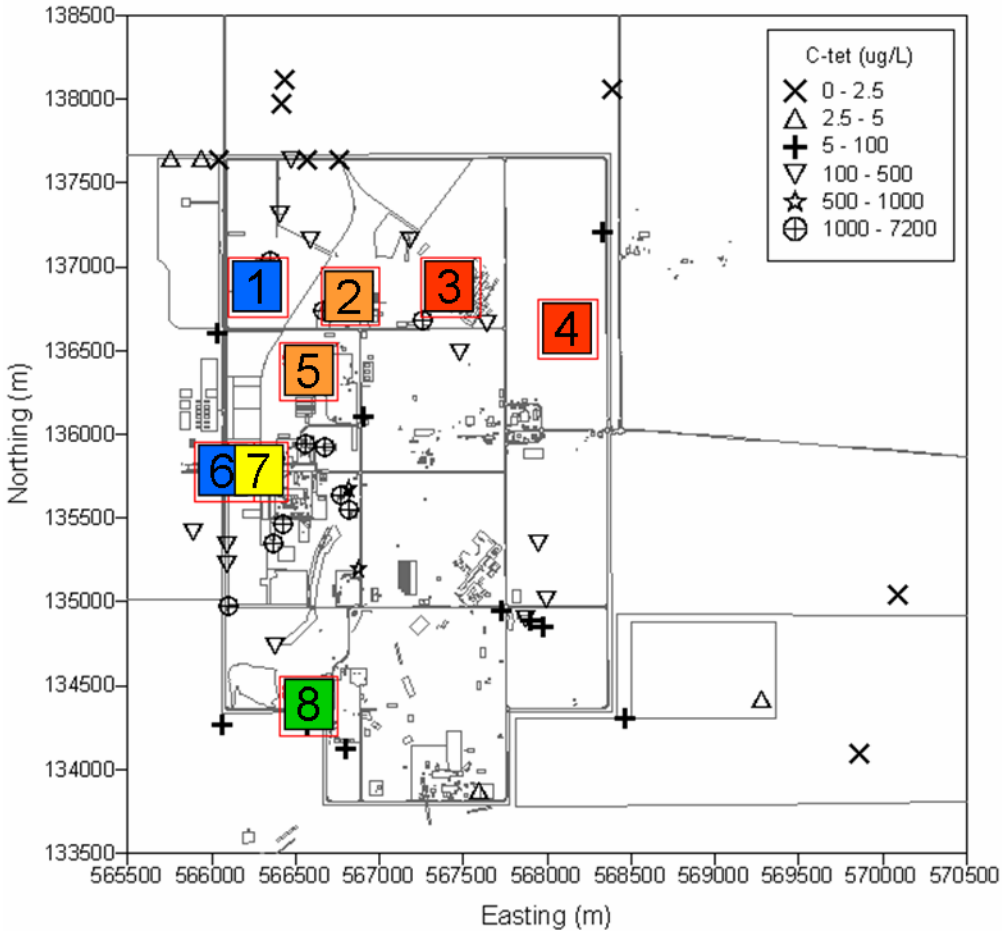

Figure 1.14. Summary Map of Classification of Sub-Areas Based on Their Likelihood of Containing Persistent Sources. Color scale ranges from red for high probability to blue for the lowest probability.

References

Deutsch CV and AG Journel. 1998. *GSLIB: Geostatistical Software Library and User's Guide*. Oxford University Press, New York.

Goovaerts P. 1997. *Geostatistics for Natural Resources Evaluation*. Oxford University Press, New York.

Chapter 2

Geostatistical Analysis of the Inventory of Carbon Tetrachloride in the Unconfined Aquifer in the 200 West Area of the Hanford Site[(a)]

Christopher J. Murray, Yi-Ju Bott, and Michael J. Truex

Summary

We performed a geostatistical analysis of two data sets. One consisted of 3D carbon tetrachloride (CT) and chloroform (CF) data from depth-discrete sampling at 192 discrete depths during drilling in 36 boreholes and is termed the depth-discrete data set. The depth-discrete data were sampled from 1999 to 2006. Plotting of the depth-discrete CT data by 10-m depth intervals shows there is significant CT at depth, especially east of the known source area. A secondary data set, termed the packer data set, also was used. It supplemented the depth-discrete data taken while drilling with 88 measurements taken in completed wells using packers in the screened intervals to attempt to isolate discrete vertical zones of the unconfined aquifer. The average concentration of the packer data set (1601 µg/L) was approximately four times higher than that of the depth-discrete data set (403 µg/L).

The depth-discrete CT data were insufficient for defining a reliable 3D variogram model, so a horizontal variogram was calculated and modeled using a normal score transform of the FY05 CT groundwater monitoring data from existing wells screened near the top of the aquifer (i.e., those data where the zone reported in the Hanford Environmental Information System (HEIS) is "TU" or "UU" or "U", or is not specified). These data also were used as supplementary data for the geostatistical mapping of both data sets. We used sequential Gaussian simulation to generate 1000 simulations of the CT and CF concentrations for the two data sets. Each simulation honors the available data, the variogram model, and the histogram of the concentration data. We used Tecplot to create a series of 3D visualizations of the median simulated CT and CF value at each node of the simulation grid as well as the probability that the CT and CF concentrations exceed several concentration thresholds. Analysis of those visualizations suggests that the lower boundary of the plume is not well defined by the simulations, with high median concentrations of CT (>100 µg/L) present at the base of the simulation grid, which is located 60 m below the top of the unconfined aquifer.

The inventory of CT and CF were estimated within the geostatistical simulation grid using a Monte Carlo approach. The inventory reflects CT and CF present in the groundwater and sorbed to the sediment, with the CF assumed to represent CT that degraded early. The inventory simulations were based solely on aqueous concentration data from the two data sets, and no dense nonaqueous phase liquid (DNAPL) is included in the inventory estimates. The Monte Carlo approach used to estimate the inventory attempted to account for uncertainty in the porosity and the sediment/water equilibrium partition coefficient (K_d) values for CT and CF by drawing values for those parameters from probability distributions.

(a) An earlier version of the geostatistical analysis presented in Chapter 2 was prepared as a letter report and issued to Fluor Hanford, Inc. on January 4, 2006.

A suite of 1000 values of the estimated CT inventory in the unconfined aquifer was generated from the 1000 simulations of CT and CF concentrations using the depth-discrete data sampled while drilling. The average value of the CT inventory for that data set is approximately 101,400 kg, and the 95% probability interval extends from 64,100 kg to 164,800 kg. The CT inventory appeared to be evenly split between the groundwater and the sediment, with a smaller amount present as CF. The CT inventory was also calculated for several concentration contours, with the highest proportion of CT associated with the 100-1,000 µg/L contour interval. We also estimated the effect of hydrolysis on the CT that entered the aquifer and calculated an average value of approximately 132,000 kg of CT that would have originally dissolved in the aquifer to account for the 101,400 kg of CT and CF that were estimated to currently reside in the aquifer.

Simulation and inventory calculations performed using the combined data set that included packer data as well as the depth-discrete data suggested inventories of CT distributed in the aquifer that were 7.4% higher, with a mean inventory of about 108,900 kg and a 95% probability interval derived from the simulations of 70,300 kg to 171,700 kg. Although a standard t-test suggests that the average inventory for the combined data set is significantly higher, there is wide uncertainty in the inventory simulations, with only a slight upward shift in the distribution of simulated inventory values.

Analysis of the potential effect of hydrolysis on CT present in the aquifer for the two data sets suggests that between 132,000 and 143,500 kg of CT would have had to reach the aquifer to result in the current distribution of CT and CF. This would account for about 18% to 19% of the 750,000 kg of CT thought to have been originally disposed of in the 200 West Area, which is almost an order of magnitude higher than previous estimates of the disposed CT accounted for by the inventory in the unconfined aquifer.

Introduction

Previous work on the carbon tetrachloride (CT) plume in the Hanford Site 200 West Area indicates that 65% of approximately 750,000 kg of CT that was delivered to the ground as a result of plutonium processing remains unaccounted for (Truex et al. 2001). We will use the value of 750,000 kg as a representative estimate of the CT release for this report. However, the quantity of CT delivered to the ground is highly uncertain, and estimates range from 577,000 kg to 922,000 kg (Rohay et. al. 1994). Previous studies have assumed that the majority of CT in the unconfined aquifer resided within the upper few meters of the aquifer. For example, Truex et al. (2001) assumed that the concentrations were greatest at the surface and declined exponentially with depth below the water table. However, recent data (e.g., Williams et al. 2005) shows that CT exists at high concentrations at significant depths within the aquifer.

To re-evaluate the inventory of CT in the unconfined aquifer in the 200 West Area, Fluor Hanford, Inc. (FH) requested PNNL to perform a 3D geostatistical study of the depth-discrete CT groundwater concentration values available in the area. An initial study was completed as a letter report to FH in January 2006, based on depth-discrete data collected during the drilling process. This chapter documents an updated version of that study, incorporating additional data available through November 2006 and also incorporating 3D concentration data from existing wells collected using packers to attempt to isolate and sample restricted depth intervals in the wells.

Methods

Depth-Discrete Data

The primary data employed in the study consisted of CT and CF data from 36 wells that had been sampled at discrete depths during drilling ("depth-discrete data set"). Concentrations were primarily from lab measurements, with field measurements only retained if laboratory measurements were not available. In addition, samples that were sampled by airlift were deleted because they might not be representative of in situ concentration values. Replicate samples from the same location and date were averaged, and all concentration values below detection were included in the analysis without change. After averaging, there were values of CT and CF concentrations available from the 36 wells for 192 discrete depths. Sampling dates for the depth-discrete data ranged from November 23, 1999, to August 4, 2006. Only the data from one well, well 299-W22-50, were from 1999-2000, with the remainder of the concentration data measured in the period from 2002 to 2006. Table 2.1 provides relevant statistics for the CT and CF data measured on those samples.

Table 2.1. Summary Statistics for Depth-Discrete Carbon Tetrachloride and Chloroform Concentration Data

FY06 3D Data	Carbon Tetrachloride (μg/L)	Chloroform (μg/L)
Mean	403.25	49.53
Standard Error	47.77	10.08
Median	88.50	5.98
Mode	2.00	2.00
Standard Deviation	661.91	139.73
Sample Variance	438123.43	19524.20
Kurtosis	6.95	29.30
Skewness	2.46	5.06
Range	3799.85	1099.93
Minimum	0.15	0.07
Maximum	3800.00	1100.00
Count	192	192
Confidence Level of Mean (95.0%)	94.22	19.89

Figures 2.1 through 2.6 show the distribution of CT and CF data for several depth intervals in the aquifer. The concentrations at each location within a given depth interval (e.g., 0-10 m below the water table [bwt]) were averaged for construction of these maps, which were generated to display the distribution of concentration data for a range of depths in the unconfined aquifer. The averaged values over those depth intervals were not used in the geostatistical analysis, which were based on the original depth-discrete data. These maps indicate that the highest CT concentration values do not always occur near the water table but are often deeper within the aquifer, especially for locations in the eastern portion of the map area. For example, in the 299-W13-1 borehole several kilometers east of the assumed source areas, the highest concentrations for both CT and CF occur in the 40- to 50-m bwt depth interval. The results shown in Figures 2.1 through 2.6 support the results already reported by Williams et al. (2005). The sample depths for 10 of the 192 samples in Table 2.1 are below 60 m bwt and occur at depths ranging from 60 to 100 m bwt.

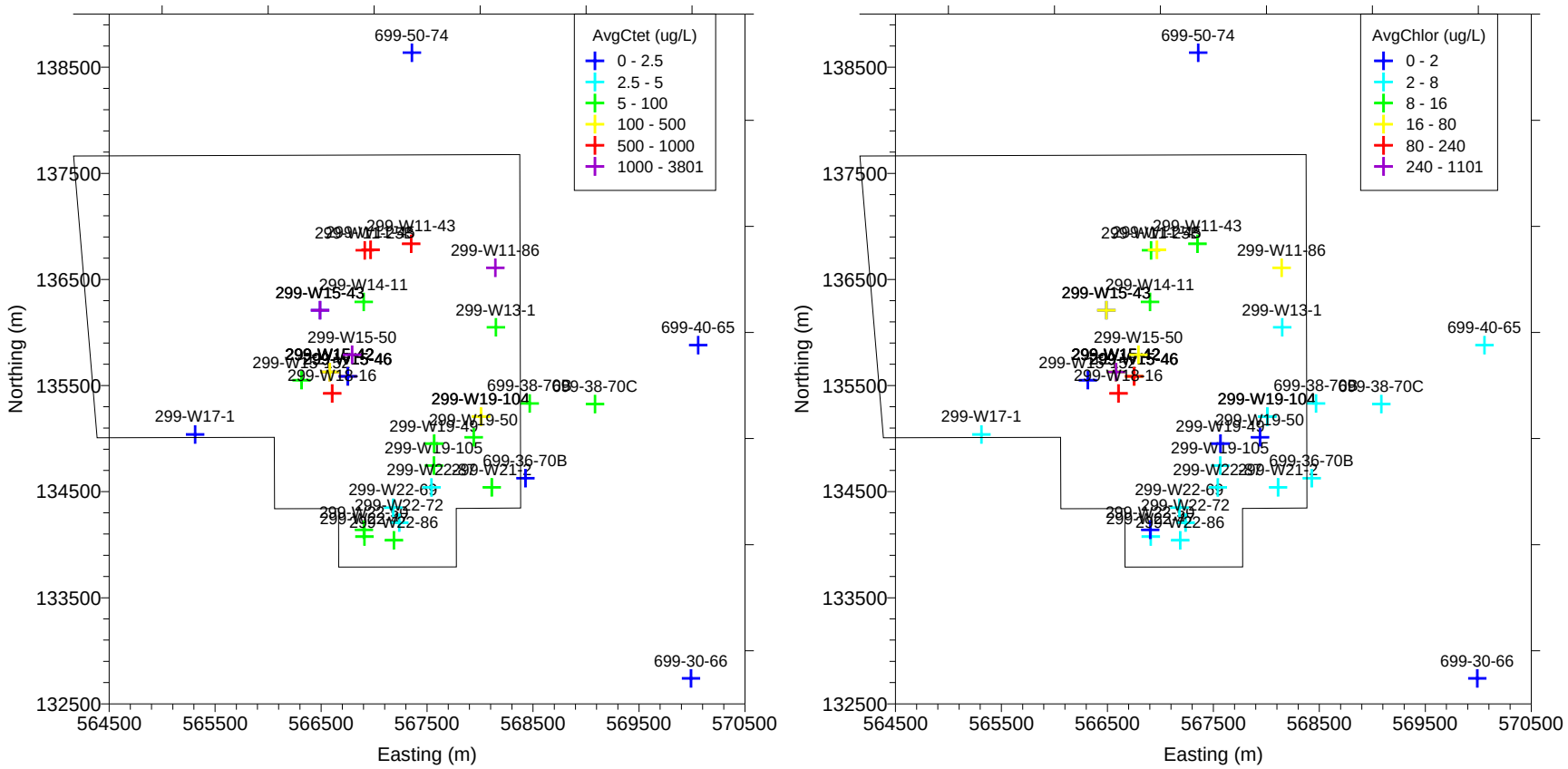

Figure 2.1. Distribution of Average CT (left) and CF (right) Concentration Data for the Interval from 0 to 10 m bwt

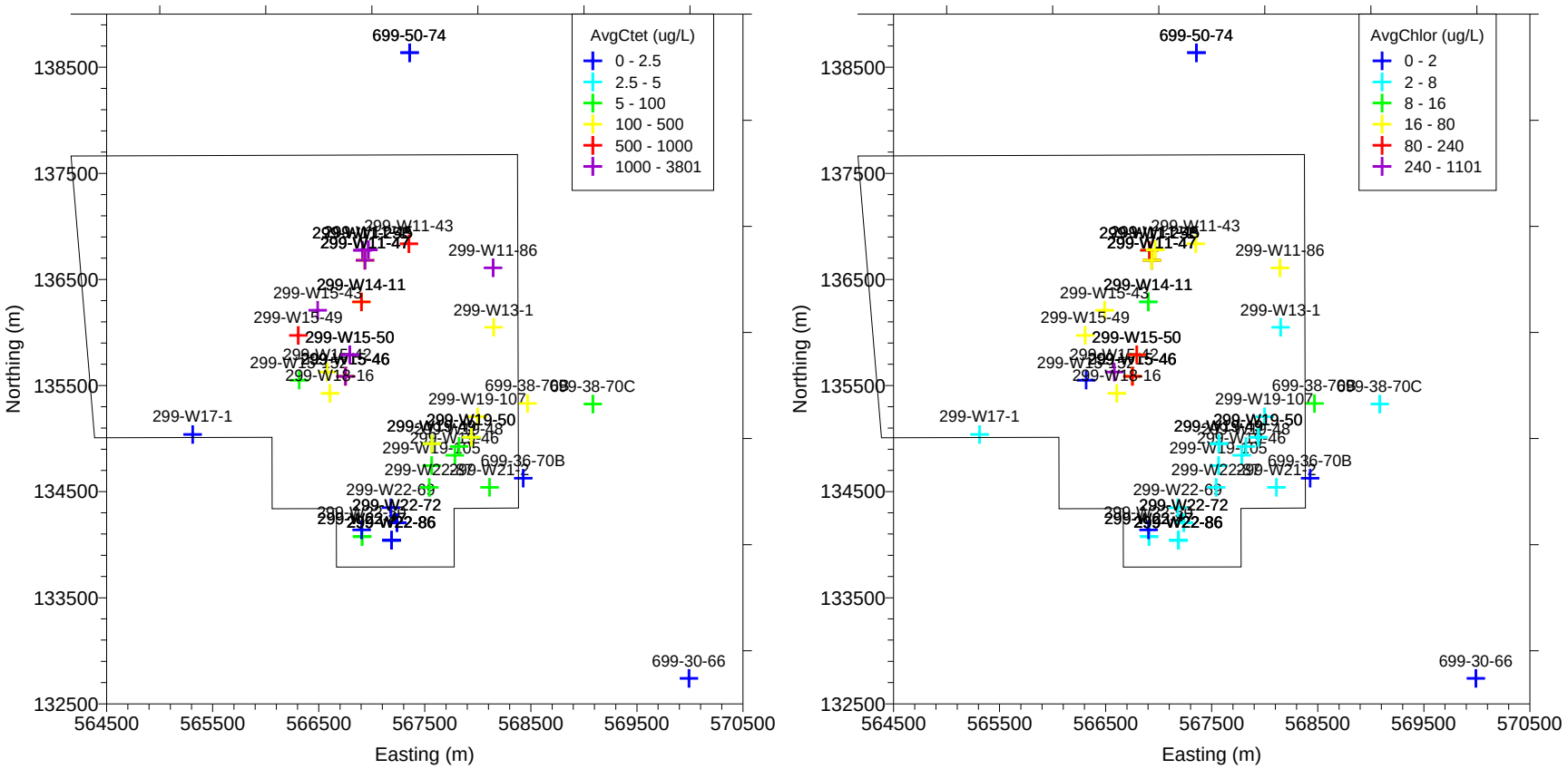

Figure 2.2. Distribution of Average CT (left) and CF (right) Concentration Data for the Interval from 10 to 20 m bwt

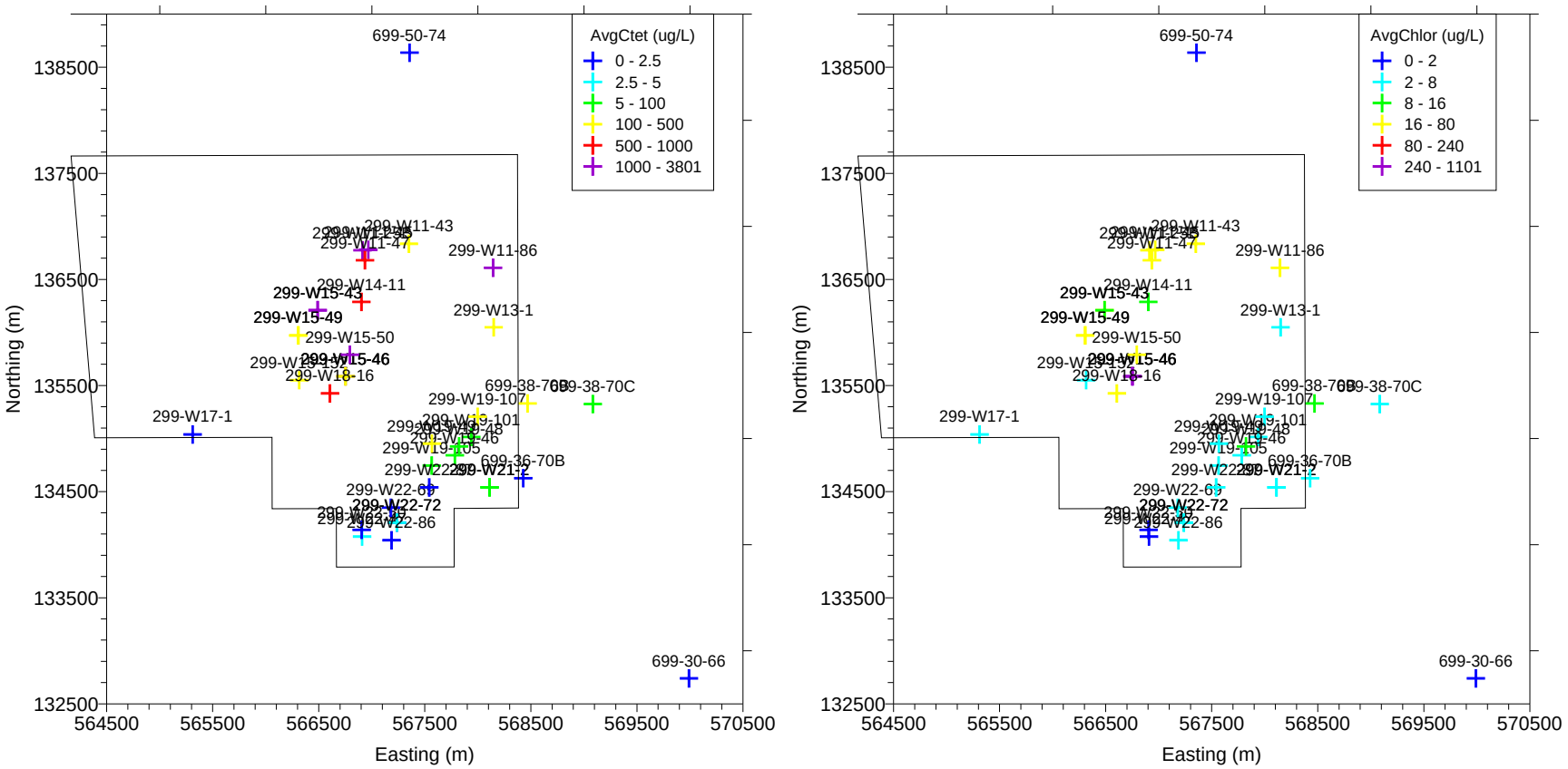

Figure 2.3. Distribution of Average CT (left) and CF (right) Concentration Data for the Interval from 20 to 30 m bwt

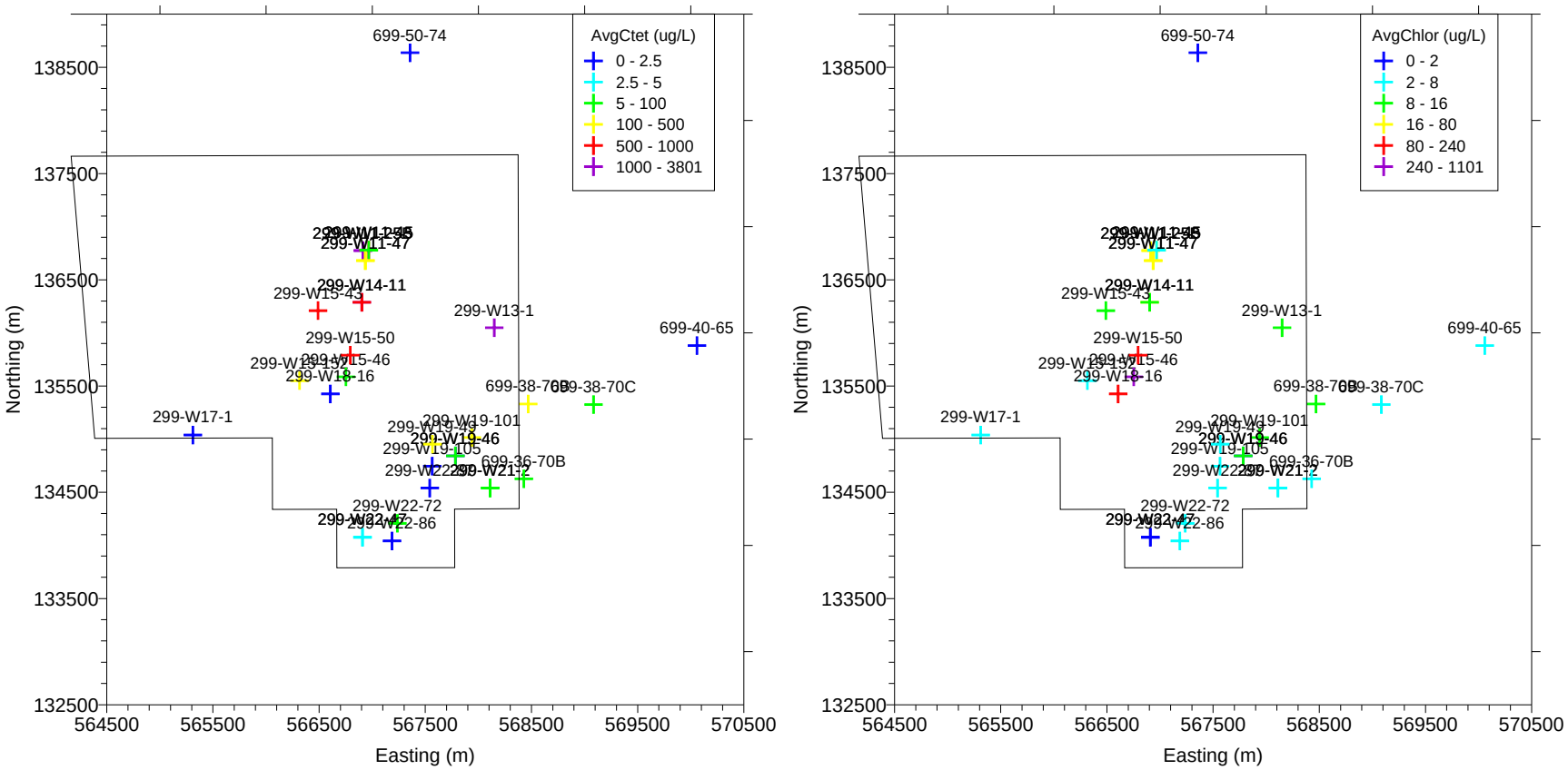

Figure 2.4. Distribution of Average CT (left) and CF (right) Concentration Data for the Interval from 30 to 40 m bwt

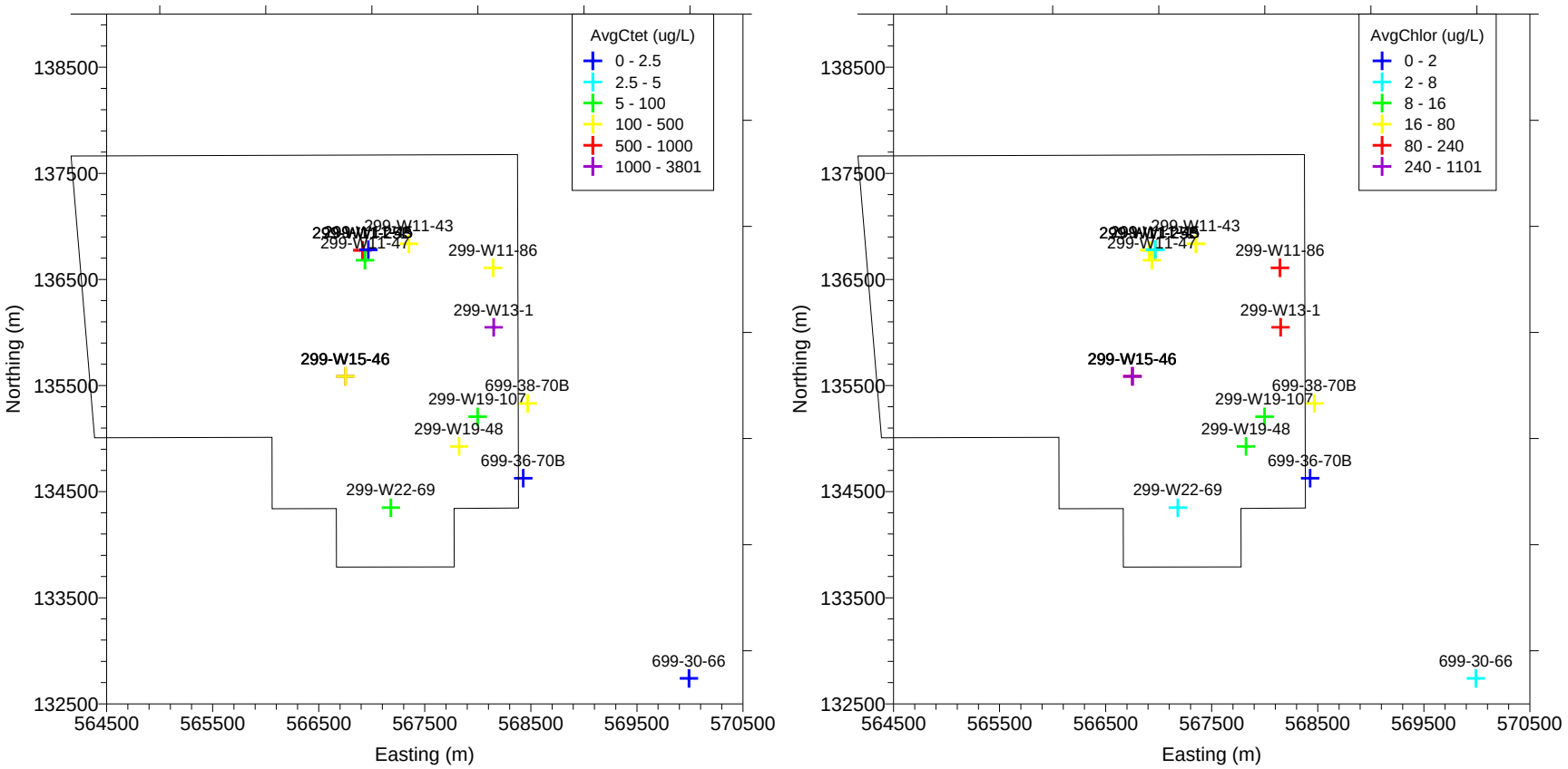

Figure 2.5. Distribution of Average CT (left) and CF (right) Concentration Data for the Interval from 40 to 50 m bwt

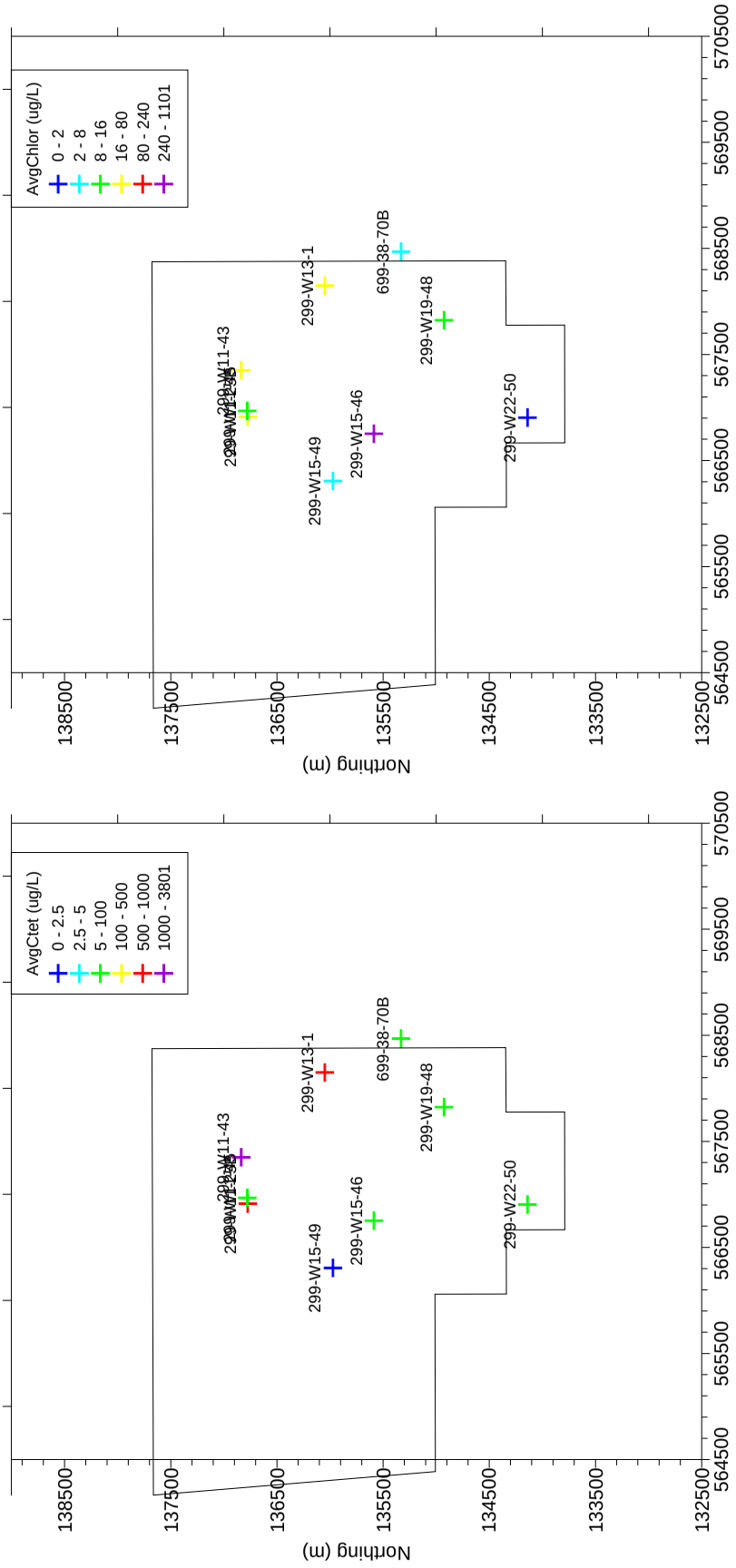

Figure 2.6. Distribution of Average CT (left) and CF (right) Concentration Data for the Interval from 50 to 60 m bwt

For the geostatistical mapping, the 3D depth-discrete CT and CF data were supplemented by a more abundant 2D data set. The 2D data were the 3-year-average CT and CF data for FY05 that were incorporated in the FY05 Hanford Site groundwater monitoring report (Hartman et al. 2006). This data set employs the standard algorithm of selecting the most recent annual average for the period from FY03 to FY05 for which data are available. The concentration values selected using those criteria (i.e., those data where the zone reported in the Hanford Environmental Information System (HEIS) is "TU" or "UU" or "U", or is not specified) are assumed to be representative of conditions in the upper portions of the aquifer (P.E. Dresel, personal communication, 2006). Figure 2.7 shows the distribution of the FY05 data relative to the boreholes where depth-discrete data were available.

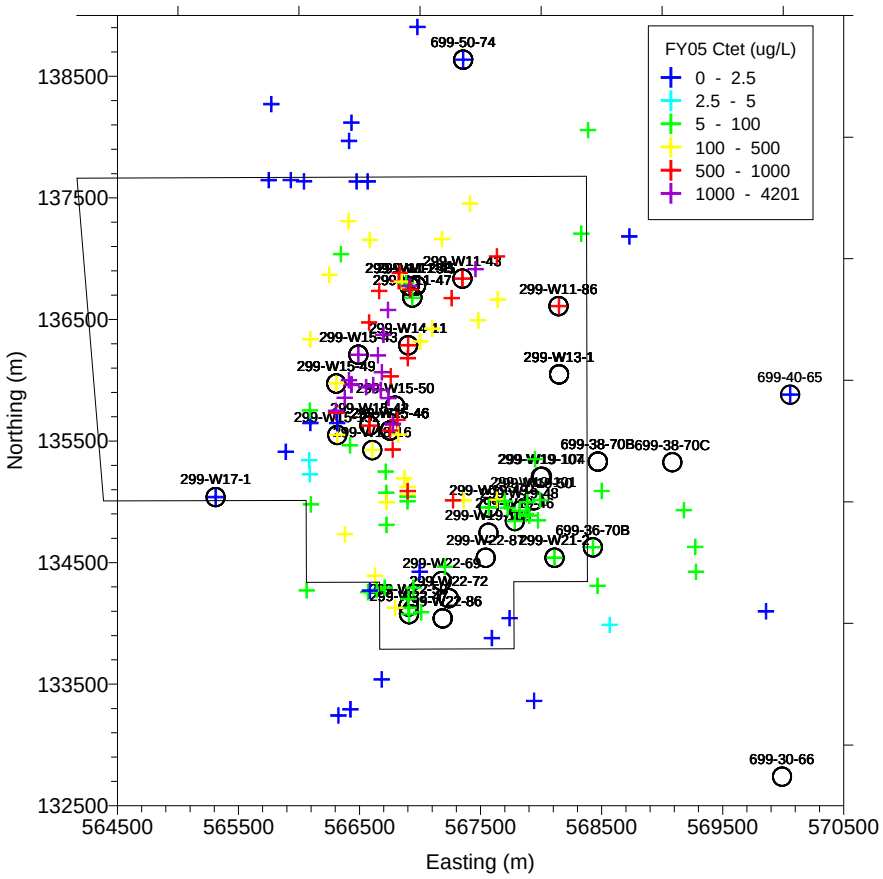

Figure 2.7. Locations of FY05 CT Data Measured Near the Top of the Aquifer and Depth-Discrete CT Locations. The depth-discrete CT locations are marked by black circles.

Packer Data

In addition to the depth-discrete data collected during drilling, we analyzed a second data set obtained by setting packers along the screened intervals in completed wells. These data, which will be referred to as the packer data set, were obtained from FH and from Vista Engineering. That data set consisted of concentration data from 88 depths in 24 wells. Data reported as below the detection limit were set to one-half the detection limit. Figure 2.8 shows the locations of the packer data relative to the

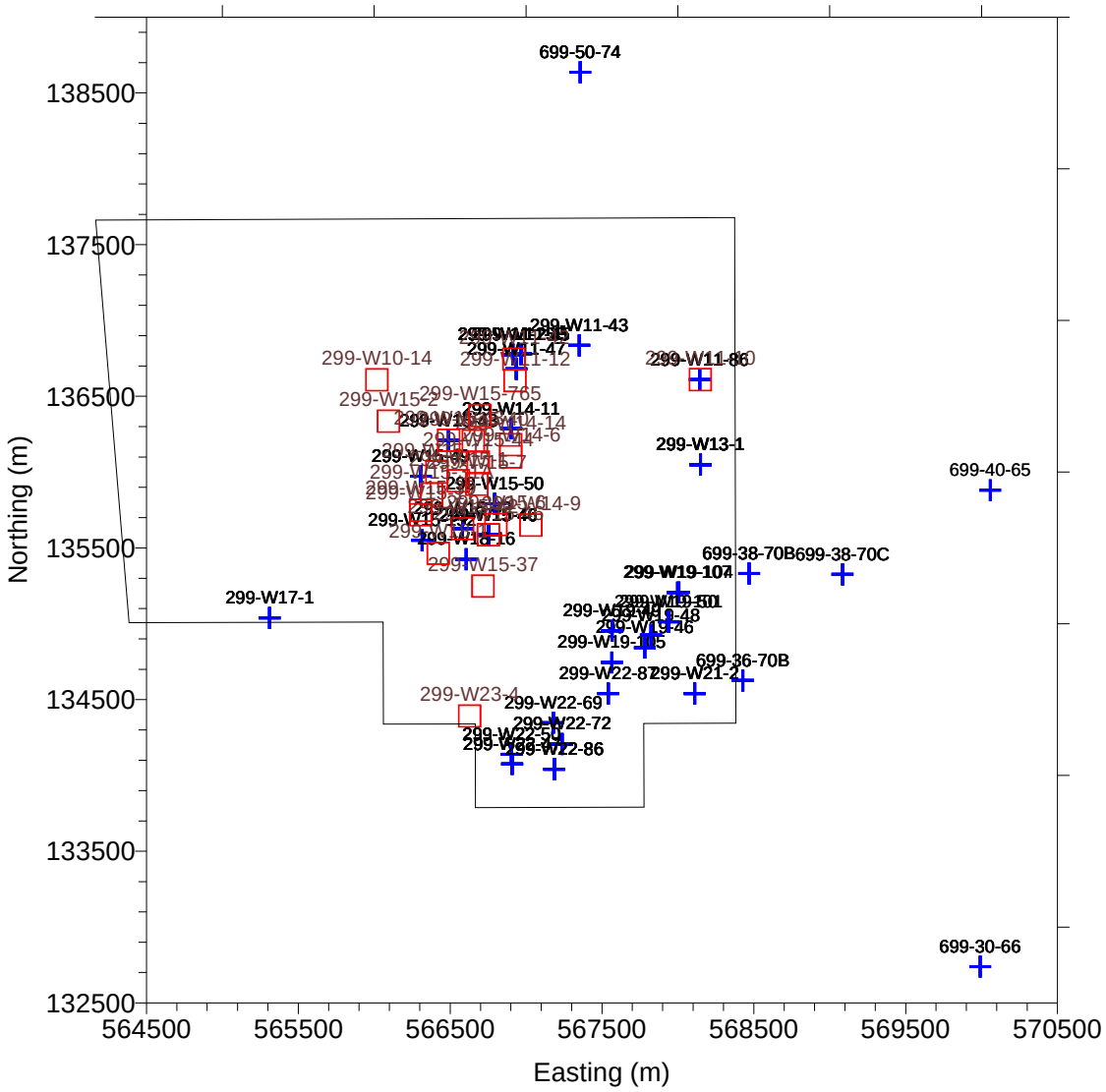

Figure 2.8. Locations of Packer Data (squares) and Depth-Discrete Data (crosses)

depth-discrete data. The vast majority of the packer data were collected in the interval from 0-10 m bwt; a relatively high number were taken also in the intervals from 10-20 m bwt and 50-60 m bwt (Table 2.2).

Most of the wells where packer data were collected were in the main high concentration area of the plume (compare Figure 2.8 and Figure 2.1). The average and median concentrations of the packer data (Table 2.3) tended to be much higher than those of the depth-discrete data. This difference is probably due to two factors. One is that many more of the well locations where depth-discrete-data were collected were on the edges of the plume and sampled lower concentrations. Another possible reason is the difference in sample collection method. The depth-discrete data sampled while drilling tend to represent a more discrete vertical sampling of the aquifer, while the collection of samples from existing wells using packers and pumping might not completely isolate water from the desired zone. This could result in mixing of high- and low- concentration groundwater in the packer samples that could, in turn, cause lower peak concentrations and higher concentrations at the low end of the range. A possible indication of the

Table 2.2. Number of Packer Data by Depth Intervals

Interval (m bwt)	(0,10)	(10,20)	(20,30)	(30,40)	(40,50)	(50,60)
Number	58	14	3	4	1	8

Table 2.3. Summary Statistics for Packer CT and CF Concentration Data

Packer Data	CT (ug/L)	CF (ug/L)
Mean	1601.27	21.63
Standard Error	139.96	4.59
Median	1500.00	15.00
Standard Deviation	1312.97	43.01
Sample Variance	1723885.64	1849.97
Kurtosis	-0.39	24.92
Skewness	0.61	4.99
Range	5099.50	269.50
Minimum	0.50	0.50
Maximum	5100.00	270.00
Count	88	88
Confidence Level of Mean (95.0%)	278.19	9.11

results of mixing can be seen in Figure 2.9, which presents depth-discrete and packer data from well 299-W15-42. In the plot of the depth-discrete data, we see a single high measurement of CT at a depth of 5.7 m below the water table (2800 μg/L) and all other measurements less than 500 μg/L. The packer data, which were collected at similar depths, suggest that all concentrations exceed 1000 μg/L and that the maximum concentration is less than 2000 μg/L. One scenario that could explain the differences between the data sets is incomplete isolation of the vertical sample zones by the packer system, giving rise to mixing of high- and low-concentration groundwater within the well bore. Given the 3-year time difference between the two sampling events, though, another possible explanation is a change in concentration patterns with time. Another potential complicating factor is the operation of the 200-ZP-1 Operable Unit groundwater pump-and-treat system, which exerts a strong influence on groundwater flow in the central part of the 200 West Area (Hartman et al. 2006) and may have modified the concentration distribution in the well during the 3-year time difference between measurements. The optimal choice for data analysis in a study like this would be to use data gathered using a single method and collected at the same time. However, the extreme scarcity of 3D concentration data in both space and time in the study area for data collected using either of the sampling methods suggested that reliance on either data set by itself would not be best. Given the relatively small area covered by the packer data in particular, the packer data and the depth-discrete data were pooled for a geostatistical evaluation of the CT inventory based on the combined 3D data sets.

The geostatistical method used for the study was sequential Gaussian simulation (Goovaerts 1997). That method is based on use of a normal score transform of the data that transforms the data so that they are normally distributed with a mean of zero and a variance of 1. This transform, which is similar in its effect to a logarithmic transform, adjusts for the positively skewed nature of the CT concentrations, but has several advantages over a logarithmic transform. Variograms of the normally transformed CT and CF data were calculated and used to estimate a model for the spatial continuity of the data. The variogram models were in turn used as input to the sequential Gaussian simulation program, SGSIM (Deutsch and Journel 1998). Two suites of 1000 simulations of the CT concentration and two suites of

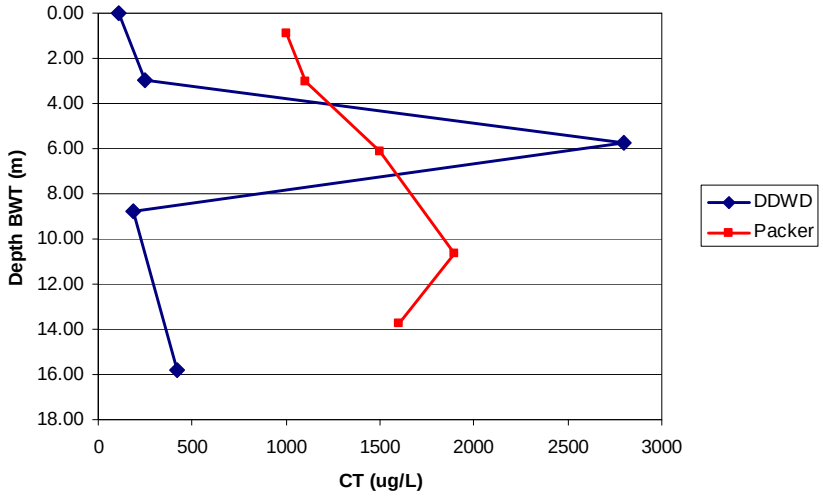

Figure 2.9. Plot of CT Data for Well 299-W15-42. The curve labeled DDWD corresponds to the depth-discrete samples collected while drilling. The curve labeled Packer represents data collected by pumping the well using packers to attempt to isolate vertical zones in the well.

1000 simulations of the CF concentration were generated, one for the depth-discrete data, and the second for the depth-discrete data combined with the packer data. The simulations were generated using a rectangular grid with spacing of 100 m in the easting and northing directions and a vertical grid spacing of 2.5 m. The coordinates of that grid extend from an easting of 564500 m to an easting of 570500 m, and between northing coordinates of 132500 m and 139000 m. The simulation grid extended to a depth of 60 m below the top of the water table. The vertical thickness of the simulation grid was chosen for two reasons. One is that the average thickness of the unconfined aquifer in the study area is approximately 60 m (Williams et al. 2005). In addition, the number of data decreases with increasing depth below the top of the aquifer, as shown in Figures 2.1 through 2.6; below a depth of 60 m, there were only two to four data points present in each 10-m interval. Each geostatistical simulation generated using this process honors the available concentration data and the variogram model and is an equally likely map of the CT or CF concentrations. Visualization of the CT and CF concentrations were generated using Tecplot, with the median simulated value at each node of the simulation grid used as a measure of the center of the distribution of simulated concentrations.

The simulations of CT and CF were post-processed using a Monte Carlo approach to provide estimates of the inventory of CT and the uncertainty in the estimated CT inventory (see Appendix for detail). For each simulation of CT and CF, the mass of CT in each cell of the 3D grid was calculated. As described previously, the simulations were performed over a rectangular 3D grid with a vertical thickness of 60 m. In some places within the study area, the unconfined aquifer is less than 60 m thick, so we used a grid of aquifer thickness (Paul Thorne, personal communication, 2006) to identify grid nodes that were deeper than the base of the unconfined aquifer and deleted the simulated inventory values associated with those grid nodes from the total inventory. Portions of the 3D grid where data were extremely sparse were blanked during the simulation process or before the calculation of the inventory.

Note that the estimated mass is based entirely on the dissolved aqueous concentrations, and does not include the mass of any CT that might be present as a dense nonaqueous phase liquid (DNAPL). The total mass calculated for the inventory included the mass of CT in the groundwater and the mass of CT sorbed to sediment, as well as the mass of CT assumed to have degraded to CF and now present in the

groundwater and sorbed to the sediment as CF. The porosity of each cell was drawn from a Gaussian distribution with a mean of 0.13 and a standard deviation of 0.033. This is the probability distribution for the Ringold Formation porosity assumed by Murray et al. (2004). Values of Ringold porosity in a range from 0.08 to 0.14 were also cited by Oostrom et al. (2006, 2007), Szecscody et al. (2005), and Thorne et al. (2006). The K_d for CT and CF were used to estimate the amount of CT and CF sorbed to the sediment in each cell, with the assumption that the CT and CF were sorbed to the fine-grained sediment in the cell. The K_d values for each simulation for CT and CF were based on Riley et al. (2005). The K_d values in that study are desorption K_ds that tend to be somewhat higher than the K_ds reported by Cantrell et al. (2003). The maximum and minimum K_d for each variable were used to estimate the maximum and minimum parameters for triangular probability distributions, with the most probable value for the distributions set to the average of the minimum and maximum. For the inventory calculations, 1000 values were drawn from the K_d probability distributions, one for each simulation. The total CT associated with each cell was accumulated for each simulation to arrive at a total current CT inventory for each simulation. The 1000 simulated CT inventory values provide the basis for an estimate of the inventory and the uncertainty associated with that estimate. In addition, the amount of the CT inventory associated with several contour intervals (CT concentrations of 5-100 µg/L, 100-1000 µg/L, 1000-4000 µg/L, and >4000 µg/L) was also calculated for each simulation.

The effect of hydrolysis, which transforms CT directly to CO_2, on the CT that originally entered the aquifer was also estimated, based on several assumptions. According to Truex et al. (2001), the disposal of CT took place from 1955 to 1973. Oostrom et al. (2004) indicate that the average time for transport of CT to the aquifer was 9 years, so we assumed the majority of the CT entered the aquifer between 1964 and 1982. We assumed an average date of 1973, so that the CT entered the aquifer 31 years or 11,315 days before 2004 (used as the representative date of depth-discrete CT data collection), at which time degradation of the CT by hydrolysis began. Truex et al. (2001) provide the parameters for a triangular probability distribution for the abiotic degradation rate due to hydrolysis (K_a), assuming a minimum half-life of 36 years, a maximum of 290 years, and a most probable half-life of 100 years. We drew 1000 values of K_a from that probability distribution and used those values to estimate the original mass of CT that entered the aquifer by applying the K_a value to the CT currently present in the aquifer (i.e., not including CT that degraded to CF) and then added that to the amount of CT that degraded to CF.

Results

Variogram Modeling

Variogram analysis of the 3D data did not produce reliable variogram models due to the relatively sparse distribution of the 3D data. There were 36 well locations for the discrete depth data, with an average of less than six observations per well, which were not sufficient to represent the experimental 3D variogram. The more widely distributed FY05 2D data from the top of the aquifer were used to calculate isotropic 2D experimental variograms for CT and CF, shown in Figure 2.10, and isotropic 2D variogram models were fit to the experimental variograms. Both variables have a relatively small nugget effect and were fit using spherical models with a correlation range of 1200 to 1300 m. Note that in both cases, the sill of the variogram model for the normal scores was set so that it levels off at a value of 1.0, which is required by the sequential Gaussian simulation algorithm. The increase in the experimental variogram values above the model sill of 1.0 for distances greater than the range, which causes an apparent poor fit for longer

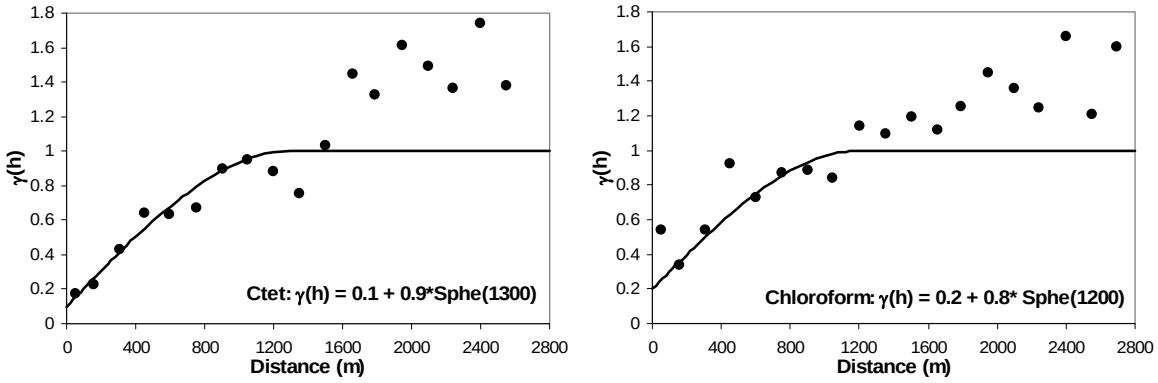

Figure 2.10. Variograms of CT and CF Calculated for 2D FY05 Average Data. Dots represent experimental variogram values, with the solid line representing the variogram models fit to the experimental variograms.

distances, is caused by the presence of spatial trends in the concentration data. Ordinary kriging was used in the simulation process to account for the presence of the trend, as recommended by Journel and Rossi (1989). Examination of cross sections produced by Williams et al. 2005 and examination of well data suggested that the plume thickness averages about 30 m, so a vertical range of 30 m was used for the 3D variogram model, which was assumed to have geometric anisotropy (i.e., the sill in the horizontal and vertical directions were assumed to be the same).

Depth-Discrete Data Taken While Drilling

We used SGSIM to generate 1000 simulations of CT and CF from the depth-discrete concentration data taken while drilling. These simulations provide 1000 simulated values of the CT and CF concentration for every node in the 3D grid. One useful way to summarize the concentrations is to calculate the median simulated value at each grid node for both CT and CF. The median simulated values were then visualized using Tecplot. Figures 2.11 and 2.12 present cutaway 3D visualizations of the median CT and CF concentrations. The cutaway is approximately through the main N-S and E-W centers of the plume. Further visualization of the plume is provided by a series of horizontal slices through the median CT concentration grid. Figures 2.13 through 2.15 present six horizontal slices at 10-m increments through the grid, from depths of 5 to 55 m below the water table.

Note that the median concentrations exceed 100 µg/L over a fairly large area at the base of the simulation grid, which extends 60 m below the top of the aquifer. This indicates that the lower limits of the plume are not well defined by the simulations, which are constrained by the extreme sparsity of data at depths that are greater than 60 m below the top of the aquifer. At least two wells, 299-W15-46 and 299-W13-1, have data with high concentrations below that depth, with the deepest data point from well 299-W13-1 having a CT concentration of 132 µg/L at a depth of 72.5 m.

Using the set of simulations, we also calculated 3D probability maps to estimate the probability of exceeding several CT concentration cutoffs at each grid node. The probability maps indicate a high probability of encountering high CT concentrations deep in the aquifer, especially in the eastern portion of the area (Figure 2.16).

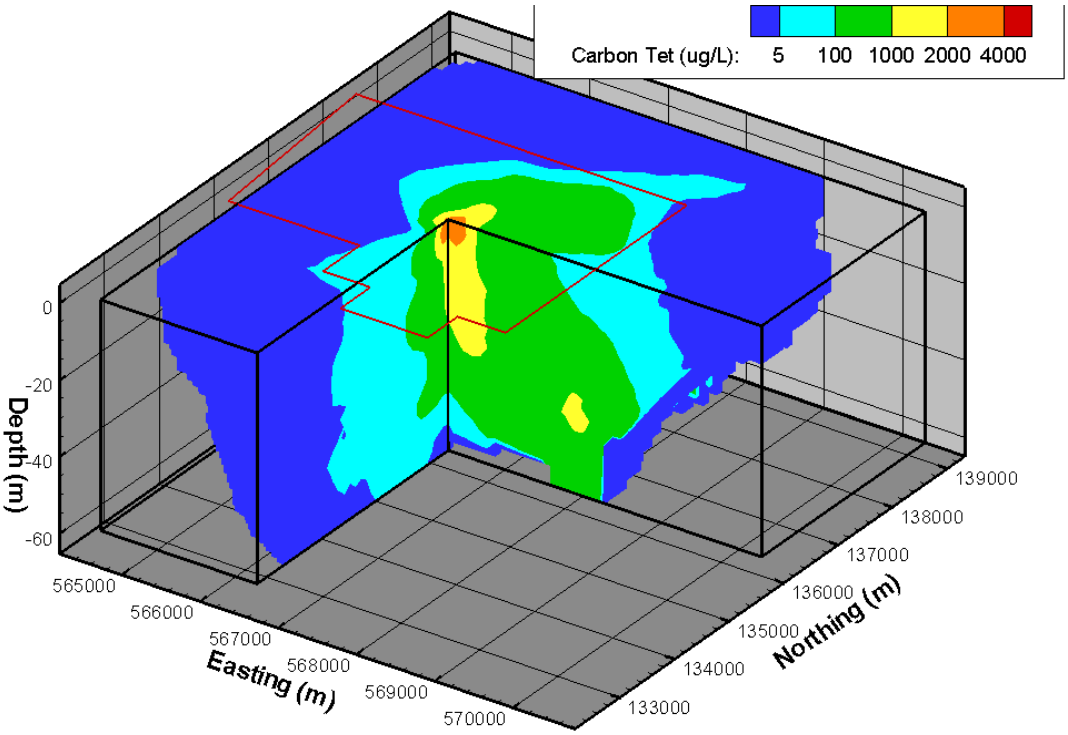

Figure 2.11. Median CT Concentrations Through Main Area of the CT Plume. Cutaway at Easting from 566500 to 570500 m and Northing from 132500 to 136000 m. Note large vertical exaggeration of approximately 50:1.

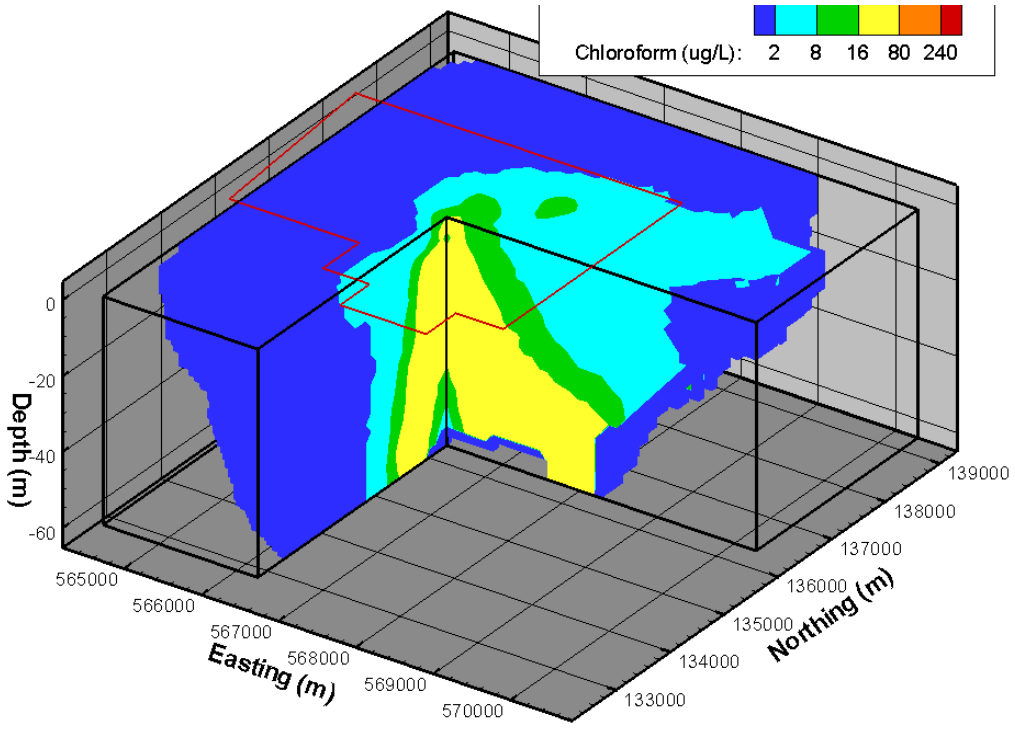

Figure 2.12. Median CF Concentrations Through Main Area of the CT Plume. Cutaway at Easting from 566500 to 570500 m and Northing from 132500 to 136000 m. Note large vertical exaggeration of approximately 50:1.

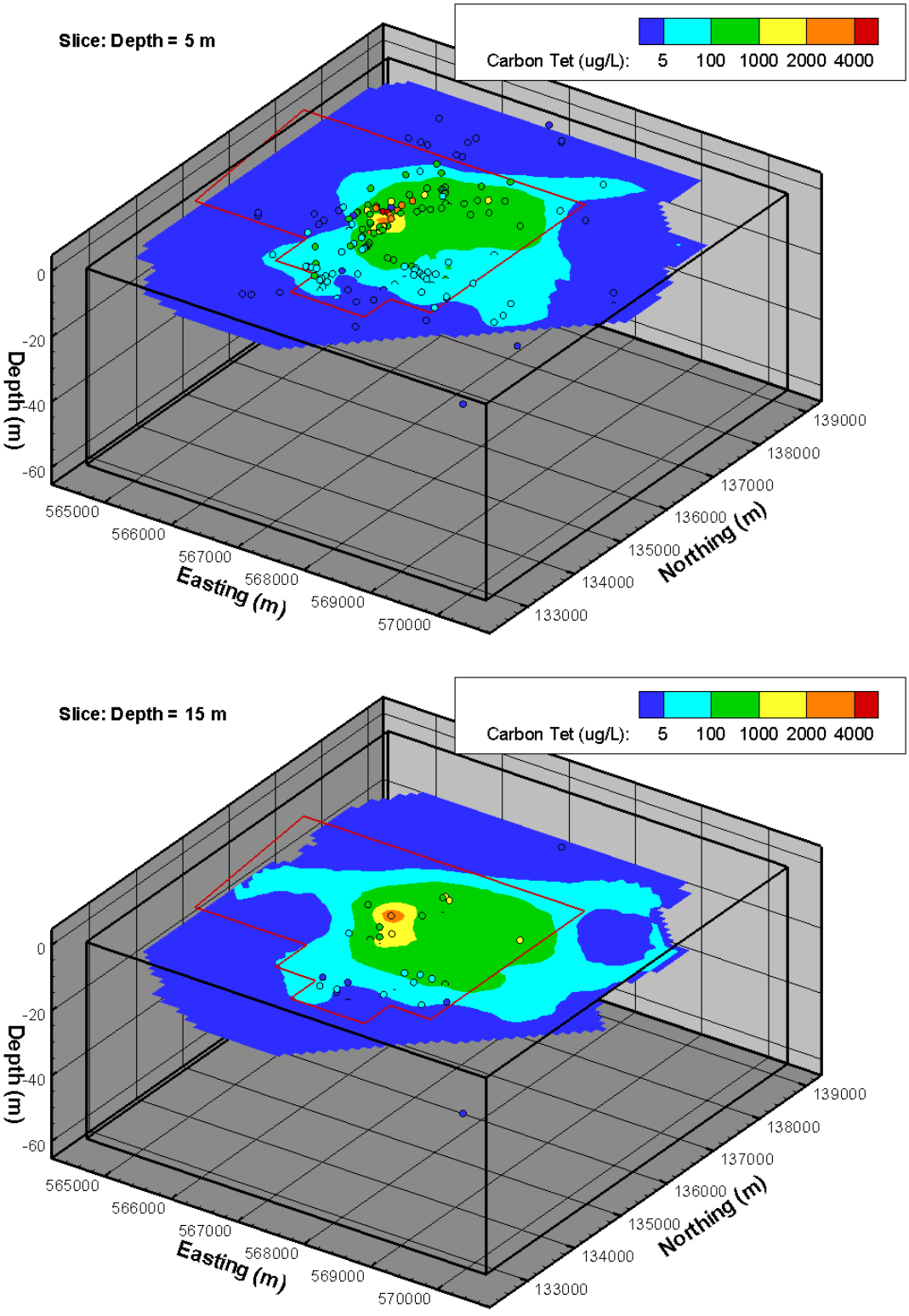

Figure 2.13. Horizontal Slices of Simulated Median Concentrations of CT at Depths of 5 m and 15 m

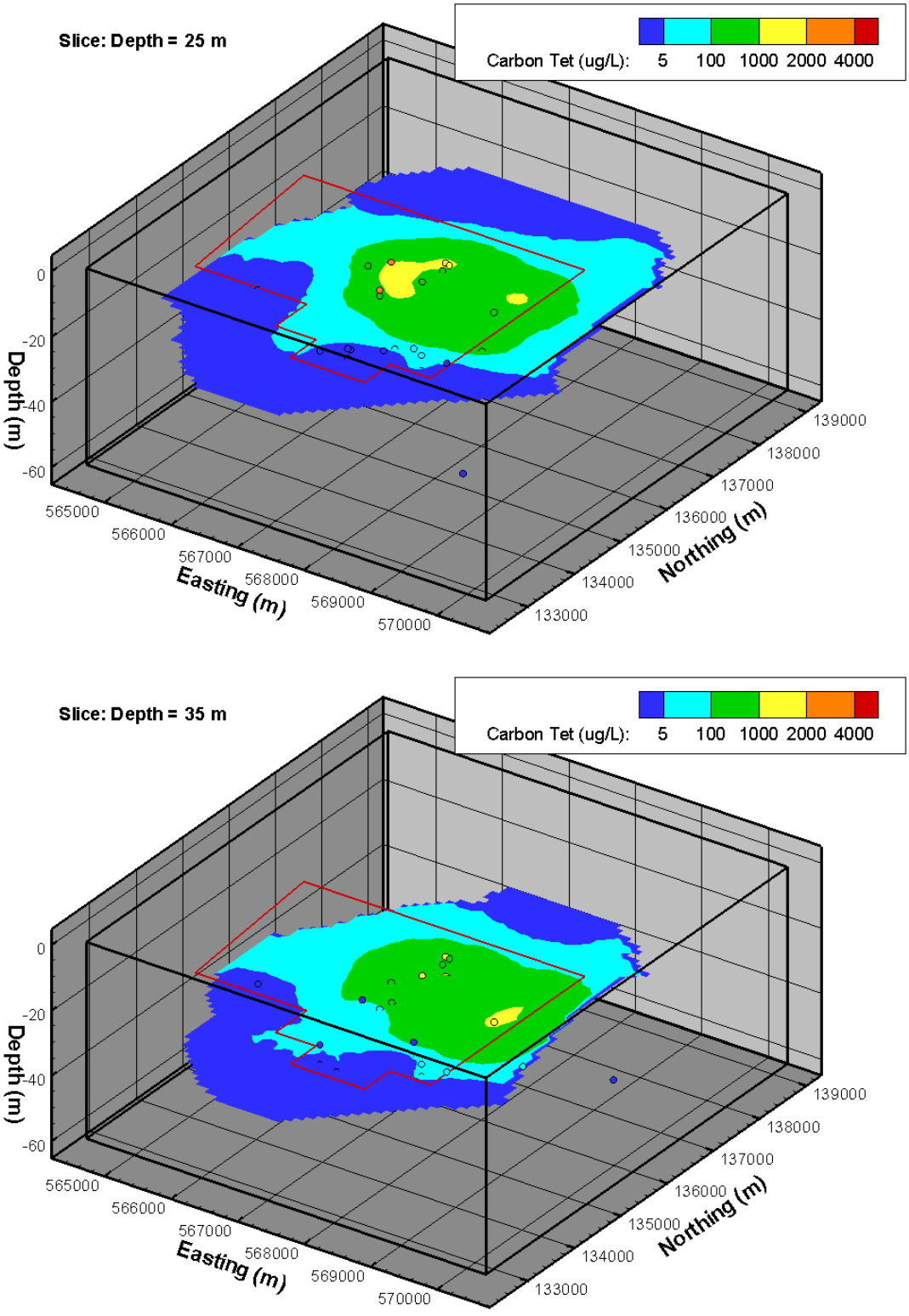

Figure 2.14. Horizontal Slices of Simulated Median Concentrations of CT at Depths of 25 m and 35 m

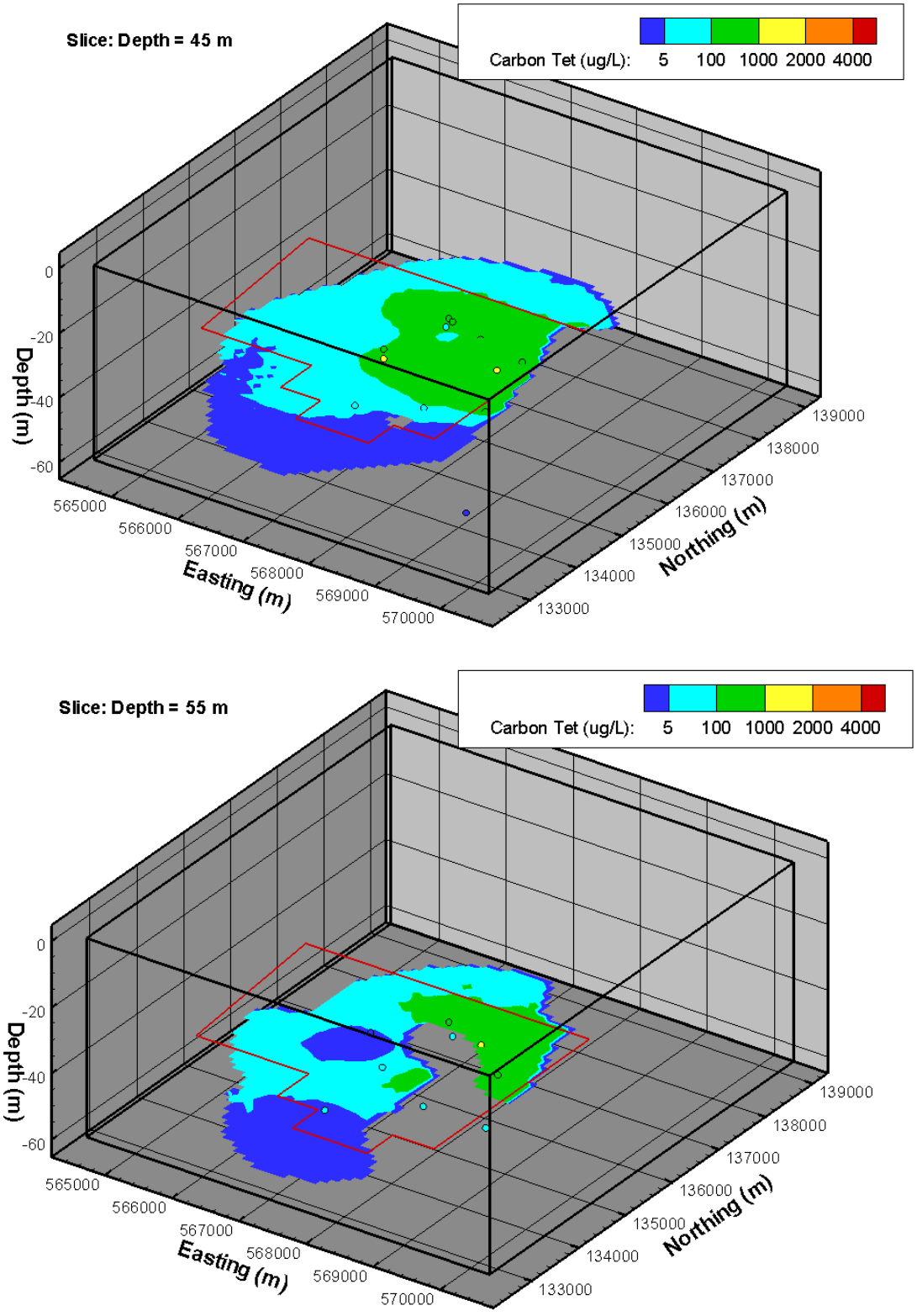

Figure 2.15. Horizontal Slices of Simulated Median Concentrations of CT at Depths of 45 m and 55 m

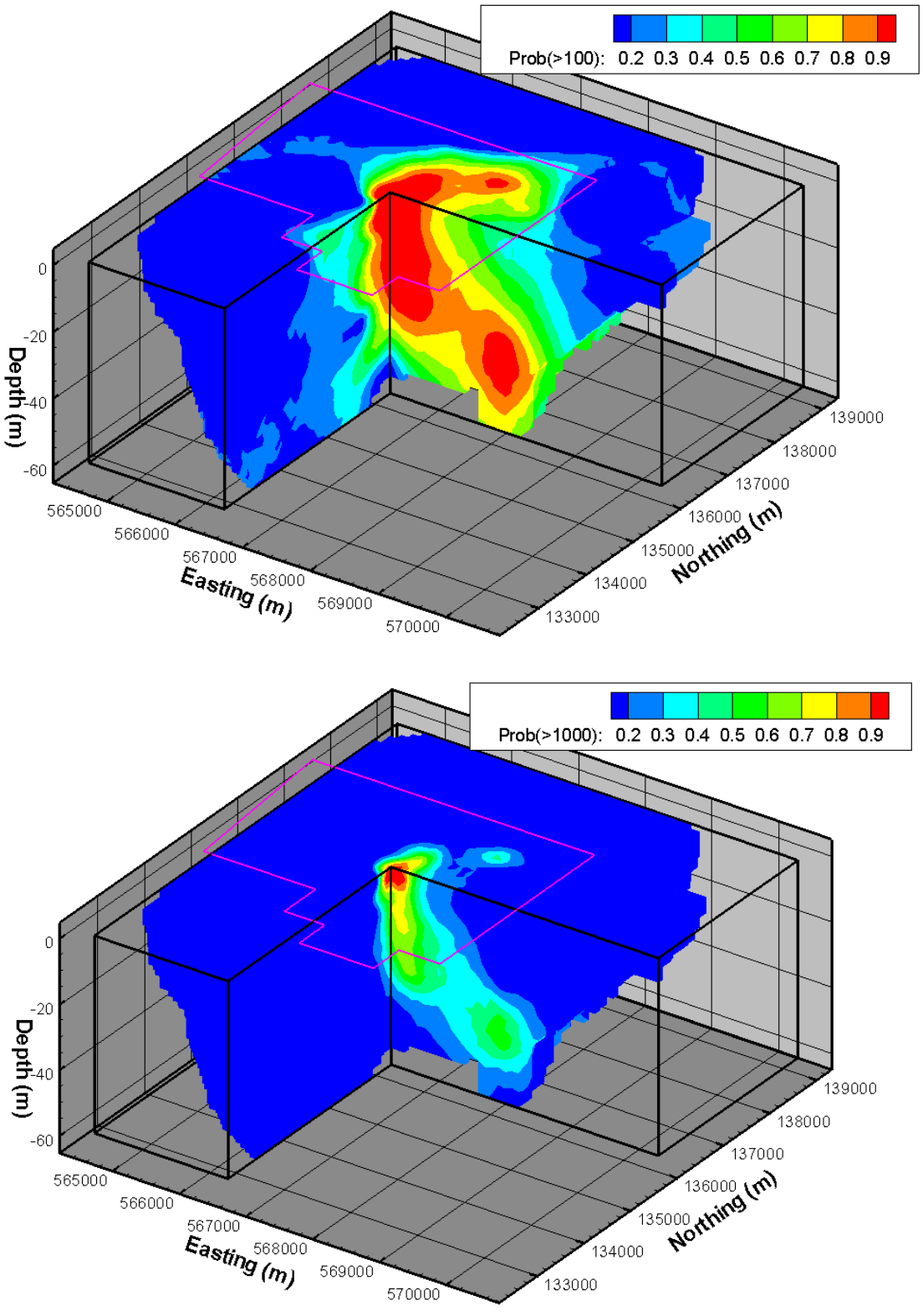

Figure 2.16. Probability That CT Concentration Exceeds 100 µg/L (upper) and 1000 µg/L (lower)

Using the approach discussed earlier and described in detail in the Appendix, the CT and CF concentration simulations were processed to provide estimates of the CT inventory present in the aquifer, both in the groundwater and sorbed to the aquifer sediment. The CF present in the groundwater and sorbed to the aquifer sediment has been converted stochiometrically to CT. Figure 2.17 is a histogram of the resulting total CT inventory currently present in the system, with summary statistics for the distribution of CT inventory values. Table 2.4 contains the summary statistics for the total inventory as well as a breakdown of the inventory by CT concentration levels. The results indicate that the mean CT inventory in the study area is approximately 101,400 kg, with a 95% probability interval of 64,300 kg to 164,100 kg. This estimate for the CT inventory in the unconfined aquifer is about 13.5% of the 750,000 kg estimated to have been disposed of in the area (Truex et al. 2001). This estimate is about 7 times larger than previous estimates of the amount of CT present in the aquifer, which were previously reported to be 2% (Truex et al. 2001). Analysis of the individual simulation results indicate that on average about 48% of the CT inventory is dissolved in the groundwater, 40% is CT sorbed to the aquifer sediment, and 12% is present as CF. Table 2.5 provides summary statistics on the proportion of the CT inventory associated with different CT contour intervals. The table indicates that the largest amount of the CT inventory (39%) is associated with the 100–1,000-µg/L contour interval, with 27% in the 1000–2000-µg/L interval, and 26% associated with the 2000–4000-µg/L interval.

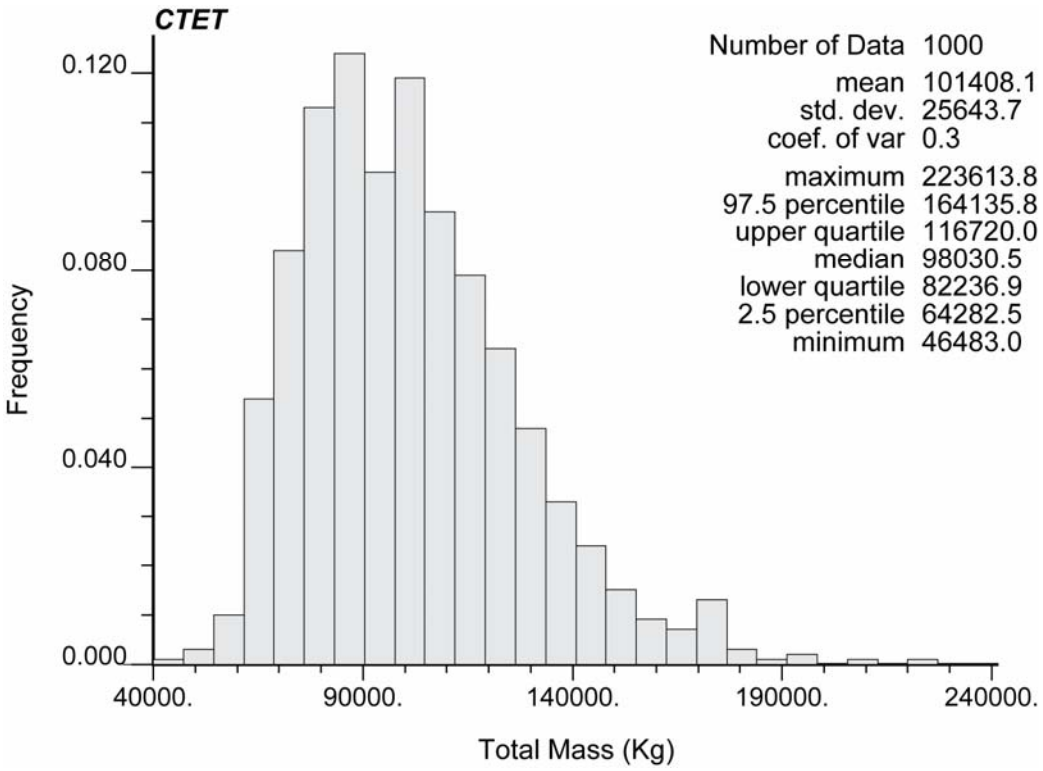

Figure 2.17. CT Inventory in the Unconfined Aquifer. Inventory reflects CT in the groundwater, sorbed to the sediment, and approximate amounts of CT that degraded to CF now present in the groundwater and sorbed to the sediment.

Table 2.4. Inventory of Total Mass and Mass Partitioned by Concentration Intervals of CT

CT Unit: Kg	Total Mass	5–100 µg/L	100–1000 µg/L	1000–2000 µg/L	2000–4000 µg/L	> 4000 µg/L
Mean	101408.0	4332.5	37880.5	26831.0	27711.7	4287.9
Standard Error	811.3	15.3	187.5	202.8	369.4	156.3
Median	98030.5	4322.7	37798.9	26243.5	25561.5	2795.4
Sample Deviation	25656.5	482.6	5930.4	6411.9	11681.2	4942.8
Kurtosis	1.0	-0.3	0.0	-0.1	1.8	17.2
Skewness	0.9	0.0	0.3	0.5	1.2	3.5
Range	177130.9	2776.1	37914.1	37105.0	76429.1	43315.5
Minimum	46483.0	2934.6	20367.2	12725.1	8470.8	323.5
Maximum	223613.8	5710.6	58281.3	49830.0	84899.9	43639.1
Count	1000	1000	1000	1000	1000	1000
97.5th Percentile	164754.2	5263.0	50575.3	41361.0	57682.9	19380.7
2.5th Percentile	64106.4	3427.2	27380.7	16647.1	11856.0	607.2
Confidence Level of Mean (95.0%)	1592.1	29.9	368.0	397.9	724.9	306.7

Table 2.5. Proportions of Total Mass Partitioned by Concentration Intervals of CT

Proportions of Total Mass: CT	5–100 µg/L	100–1000 µg/L	1000–2000 µg/L	2000–4000 µg/L	> 4000 µg/L
Mean	4.51%	38.46%	26.56%	26.38%	3.71%
Standard Error	0.03%	0.17%	0.05%	0.15%	0.10%
Median	4.44%	38.70%	26.79%	26.27%	2.80%
Standard Deviation	1.06%	5.51%	1.61%	4.82%	3.06%
Kurtosis	-0.2428	0.0537	2.9690	-0.3423	9.6074
Skewness	0.1765	-0.4065	-1.2051	0.2087	2.6231
Range	6.72%	32.88%	12.73%	25.41%	26.30%
Minimum	1.77%	19.90%	17.47%	14.23%	0.46%
Maximum	8.49%	52.78%	30.20%	39.64%	26.76%
Count	1000	1000	1000	1000	1000
97.5th Percentile	6.58%	47.86%	29.04%	36.37%	13.08%
2.5th Percentile	2.51%	26.48%	22.37%	17.57%	0.85%
Confidence Level of Mean (95.0%)	0.07%	0.34%	0.10%	0.30%	0.19%

Estimating the effects of hydrolysis on the CT present in the aquifer indicates that the current inventory of CT and CF represents an even larger proportion of the CT originally disposed of in the study area. Figure 2.18 indicates that the mean estimate of the amount of original CT represented by the current inventory is 132,000 kg. This estimates the amount of original CT that would need to have been delivered to the aquifer in order for the current inventory of CT and CF to be present (which is 101,400 kg), after accounting for the complete breakdown of a portion of the CT by hydrolysis. The estimate of 132,000 kg represents about 18% of the amount of CT estimated to have been disposed of in the 200 West Area, an estimate that is almost an order of magnitude higher than earlier estimates of the amount of the total CT accounted for by the unconfined aquifer.

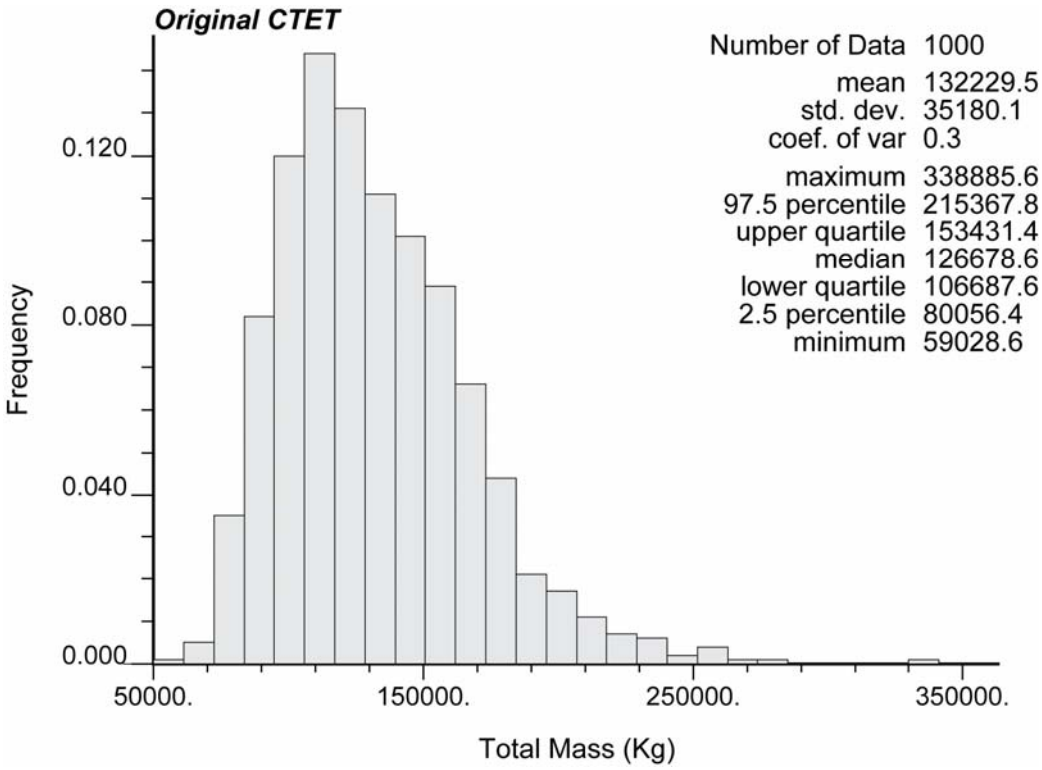

Figure 2.18. Estimated Original Total Mass of CT Present in the Aquifer Before Its Abiotic Degradation over Time by Hydrolysis

Depth-Discrete Data Combined with Packer Data

The geostatistical simulation and inventory calculation procedure described above was then applied to a combined 3D data set consisting of the depth-discrete data and the packer data. As with the depth-discrete data set, this was supplemented with the FY05 2D data collected near the top of the water table (Figure 2.19).

We used SGSIM to generate 1000 simulations of CT and CF from the combined 3D concentration data. These simulations provide 1000 simulated values of the CT and CF concentration for every node in the 3D grid. Figure 2.20 presents a cutaway 3D visualization of the median CT with the same orientation and scale as Figure 2.11. A significant difference can be seen in the main western portion of the plume, at the intersection of the east-west and north-south cutaway planes. There appears to be a substantially larger volume of the aquifer in that area that has median simulated concentrations in excess of 2000 µg/L that reach much deeper into the aquifer.

Using the set of simulations generated using the combined data set, we also calculated 3D probability maps to estimate the probability of exceeding several CT concentration cutoffs at each grid node. Significant changes can be seen also between the probability maps calculated based on the depth-discrete data (Figure 2.16) and those based on the combined data set (Figure 2.21). The probability maps that include the packer data as well as the depth-discrete data indicate a much higher probability of encountering concentrations in excess of 100 µg/L near the base of the unconfined aquifer in the main western area of the plume, near the cutaway intersection (Figure 2.21), with probabilities exceeding 70%.

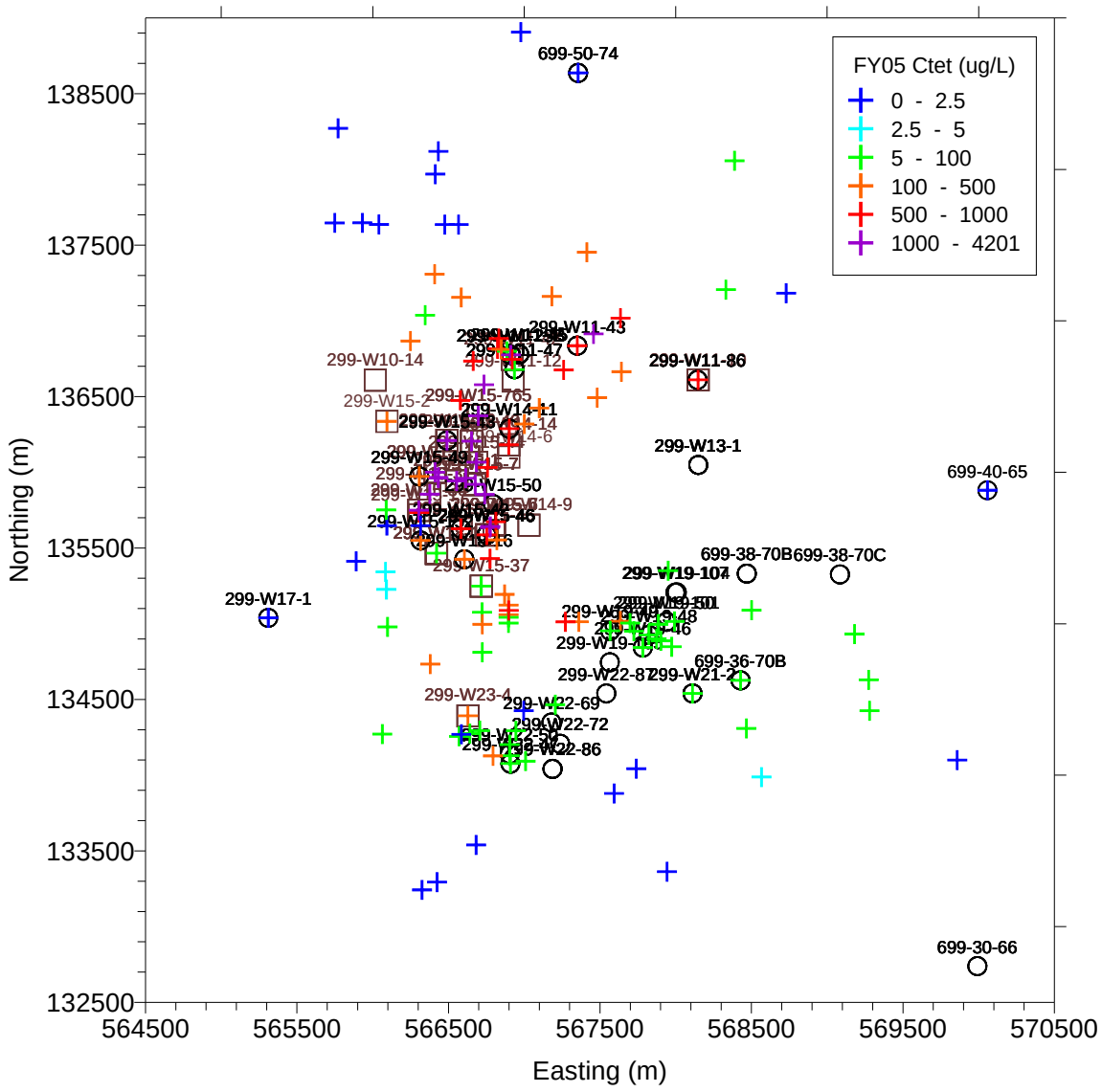

Figure 2.19. Sample Locations for Combined Data Set Consisting of Depth-Discrete Data (circles), Packer Data (squares), and FY05 Data Sampled in the Upper Portion of the Aquifer

They also indicate a higher probability of encountering high CT concentrations deep in the aquifer, greater than 1000 µg/L in that area. Comparison of the lower portion of Figure 2.21 and the lower portion of Figure 2.16 suggests that the probability of encountering concentrations in excess of 1000 µg/L near the base of the aquifer are at least double. In addition, the simulations based on the combined data indicate a much larger volume of the main plume where the probability of exceeding 1000 µg/L is almost certain (more than 90%). The lower portion of Figure 2.21 also suggests a higher probability that the high concentration zone is continuous between the western and eastern areas of the plume.

Given the increased volume of the aquifer that appears to have high concentrations of CT, it is not surprising that inventory calculations based on the combined data set are higher than those prepared using just the depth-discrete data (compare Figure 2.22 with Figure 2.17). The mean simulated inventory value

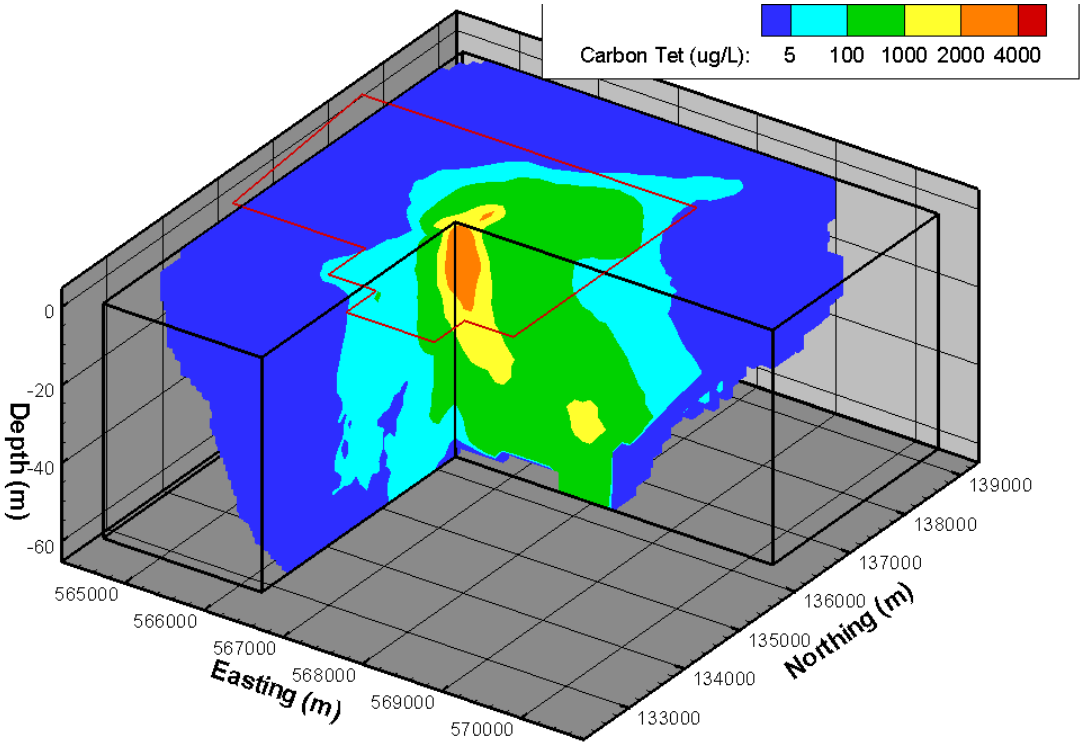

Figure 2.20. Median CT Concentrations Through Main Area of the CT Plume Based on Combined Depth-Discrete Data and Packer Data. Cutaway at Easting from 566500 to 570500 m and Northing from 132500 to 136000 m. Note large vertical exaggeration of approximately 50:1.

of dissolved and sorbed CT and chloform using the combined data is 7.4% higher, with a mean inventory of about 108,900 kg. A t-test comparing the two sets of simulated inventory values suggests that the mean values are significantly different, and the lack of overlap between the notches on Figure 2.23 also suggests that the median inventory is significantly higher for the inventory simulations generated using the combined data set. However, because of the wide variation in the Monte Carlo inventory simulations, which reflects uncertainty in many factors that contribute to the inventory values, there is almost total overlap between the distributions of simulated inventory values generated using the depth-discrete data and the combined data (Figure 2.23). A 95% probability interval for the simulated inventories based on the combined data set ranged from 70,300 kg to 171,700 kg, which is slightly higher than the 95% probability interval for the simulations generated using the depth-discrete data (64,300 kg to 164,100 kg).

Comparison of the inventory broken out by concentration levels for the combined data (Tables 2.6 and 2.7), with those generated using just the depth-discrete data (Tables 2.4 and 2.5) indicates that the majority of the difference between the two sets of inventory simulations occurs due to a decrease in the proportion of the simulated inventory occurring in the 100–1,000-µg/L concentration interval and an increase in the proportion of the inventory occurring in the 2000–4000-µg/L concentration interval in the combined data set. As suggested earlier by comparison of the probability maps, this result indicates that use of the combined data set results in a greater proportion of simulated concentration values that fall into one of the high concentration intervals (i.e., 2000–4000 µg/L).

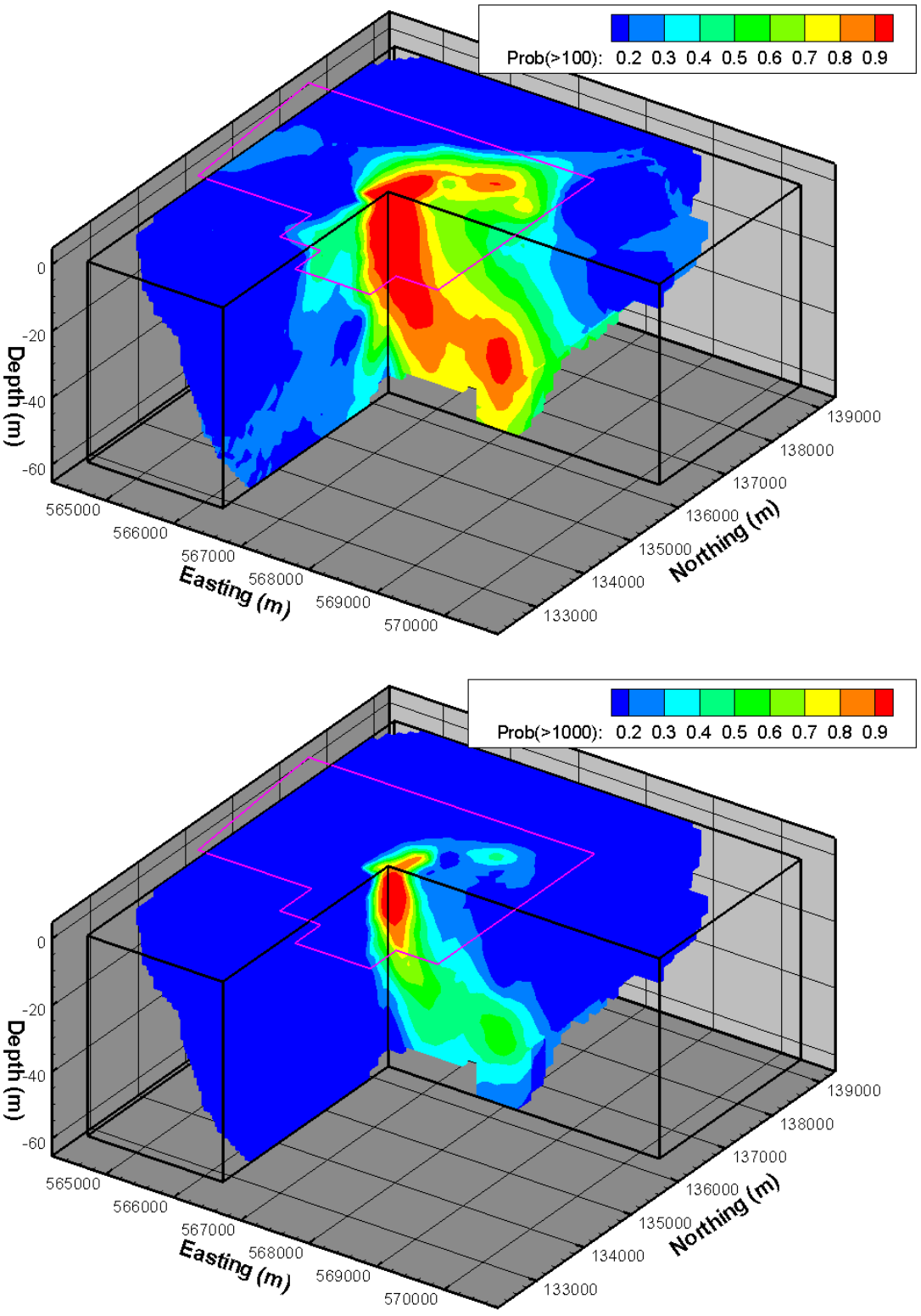

Figure 2.21. Probability That CT Concentration Exceeds 100 µg/L (upper) and 1000 µg/L (lower), Based on Combined Depth-Discrete Data and Packer Data

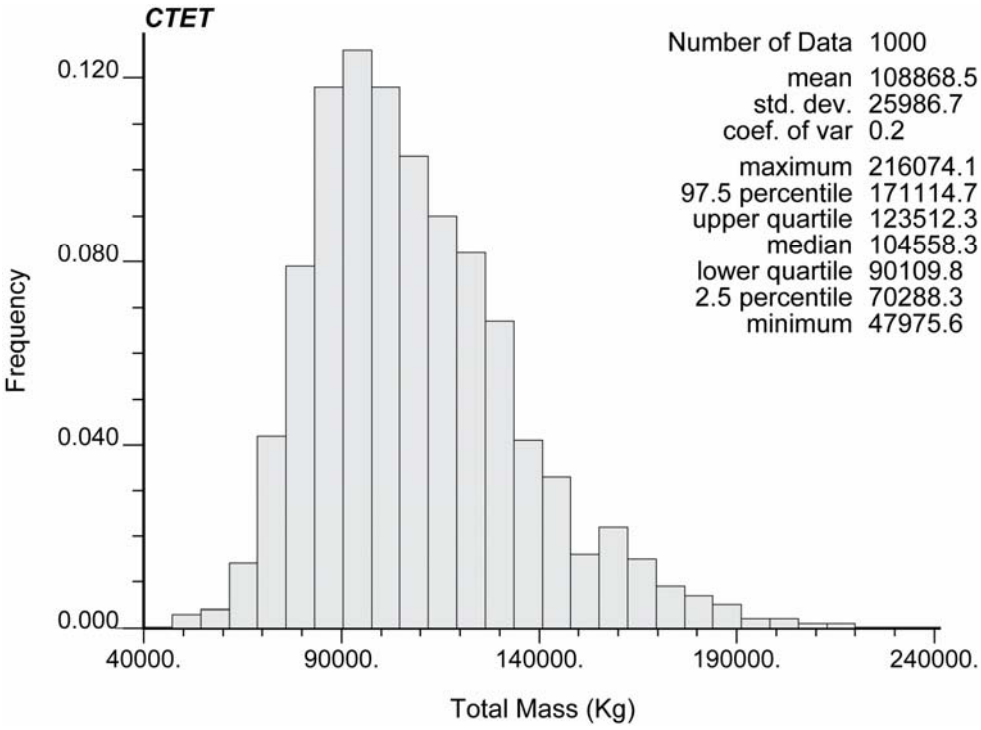

Figure 2.22. CT Inventory in the Unconfined Aquifer, Based on Combined Depth-Discrete and Packer Data. Inventory reflects CT in the groundwater, sorbed to the sediment, and approximate amounts of CT that degraded to CF that is now present in the groundwater and sorbed to the sediment.

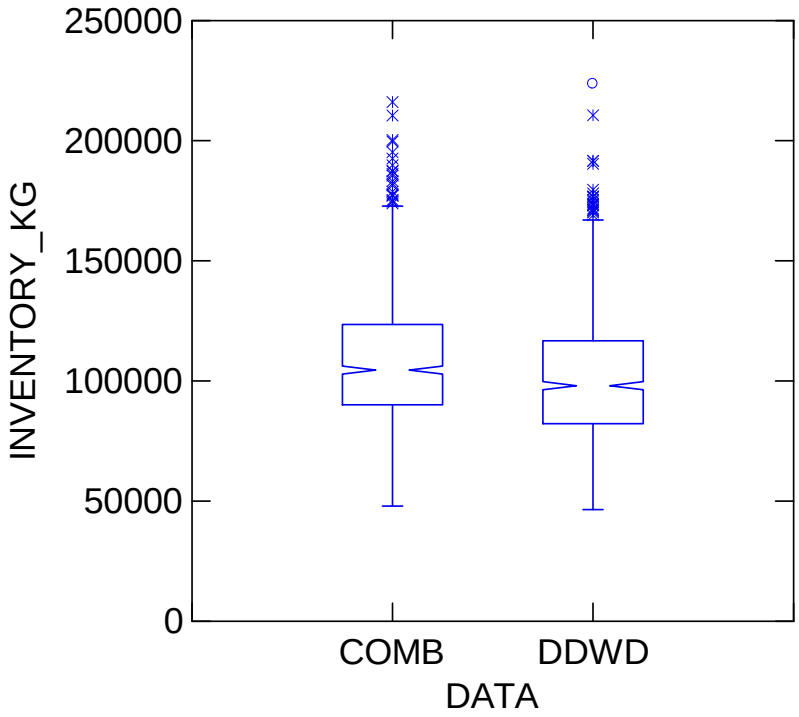

Figure 2.23. Comparison of the Simulated CT Inventory Values Generated Using the Depth-Discrete Data (DDWD) and the Combined Data Set (COMB)

Table 2.6. Inventory of Total Mass and Mass Partitioned by Concentration Intervals of CT, Based on Combined Depth-Discrete and Packer Data

CT Unit: Kg	Total Mass	5–100 µg/L	100–1000 µg/L	1000-2000 µg/L	2000–4000 µg/L	> 4000 µg/L
Mean	108868.5	4209.7	33202.3	29412.1	37159.0	4534.2
Standard Error	822.2	15.2	162.6	197.7	409.2	140.0
Median	104558.1	4205.6	32777.7	28715.3	34574.9	3143.6
Sample Deviation	25999.7	479.7	5142.8	6252.2	12940.6	4427.1
Kurtosis	0.8	-0.1	-0.1	0.1	1.1	16.3
Skewness	0.8	0.1	0.2	0.5	1.0	3.4
Range	168098.5	3152.8	29313.3	36244.2	83524.3	38501.1
Minimum	47975.6	2713.5	19735.2	13471.6	10414.8	418.5
Maximum	216074.1	5866.3	49048.5	49715.9	93939.1	38919.7
Count	1000	1000	1000	1000	1000	1000
97.5th Percentile	171664.1	5190.4	43845.9	43594.0	69989.3	17267.5
2.5th Percentile	70278.5	3293.9	23888.7	18734.5	18717.4	934.1
Confidence Level of Mean (95.0%)	1613.4	29.8	319.1	388.0	803.0	274.7

Table 2.7. Proportions of Total Mass Partitioned by Concentration Intervals of CT, Based on Combined Depth-Discrete and Packer Data

Proportions of Total Mass: CT	5–100 µg/L	100–1000 µg/L	1000-2000 µg/L	2000–4000 µg/L	> 4000 µg/L
Mean	4.04%	31.26%	27.20%	33.39%	3.77%
Standard Error	0.03%	0.13%	0.05%	0.13%	0.08%
Median	4.01%	31.35%	27.44%	33.42%	3.05%
Standard Deviation	0.87%	4.20%	1.62%	4.24%	2.60%
Kurtosis	0.1852	0.0005	2.7994	-0.3180	12.0442
Skewness	0.2726	-0.2082	-1.2257	-0.0445	2.6922
Range	5.56%	24.69%	13.40%	24.58%	25.61%
Minimum	1.80%	17.91%	17.46%	21.71%	0.61%
Maximum	7.36%	42.60%	30.86%	46.29%	26.22%
Count	1000	1000	1000	1000	1000
97.5th Percentile	5.93%	39.09%	29.68%	41.69%	10.74%
2.5th Percentile	2.42%	22.34%	23.19%	25.38%	1.19%
Confidence Level of Mean (95.0%)	0.05%	0.26%	0.10%	0.26%	0.16%

Estimating the effects of hydrolysis on the CT and CF present in the aquifer for the combined data set indicates that the current inventory of CT represents an even larger proportion of the CT originally disposed of in the study area. Figure 2.24 indicates that the mean estimate of the amount of original CT represented by the current inventory is 143,500 kg. This represents an increase of about 9% in the total estimated inventory relative to that derived using just the depth-discrete data. However, that increase in total estimated inventory results in a small increase from about 18% of the amount of CT estimated to have been disposed of in the 200 West Area based on the depth-discrete data set, to 19% based on the combined data set. In either case, the total estimated inventory is almost an order of magnitude higher than earlier estimates of the amount of the total CT accounted for by the unconfined aquifer that assumed that there was little CT at depth within the aquifer.

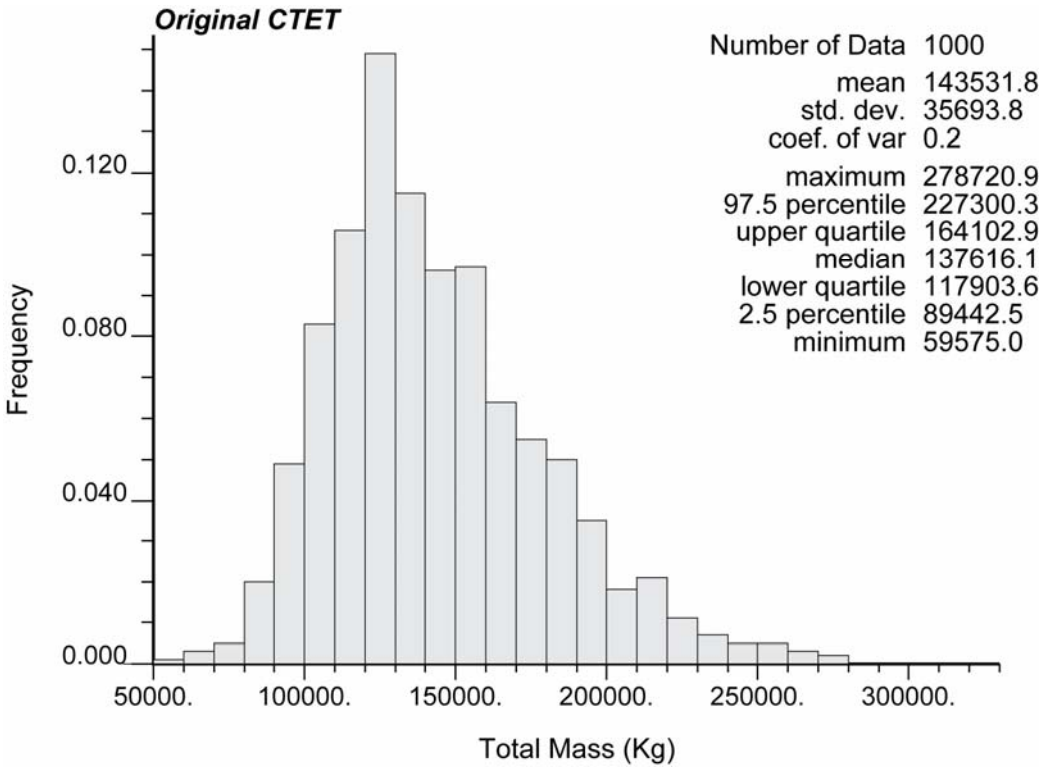

Figure 2.24. Estimated Original Total Mass of CT Present in the Aquifer Before Abiotic Degradation over Time by Hydrolysis, Based on Combined Depth-Discrete and Packer Data

Discussion

This analysis was based on geostatistical analysis of two data sets, one consisting of 3D CT and CF data from depth-discrete sampling at 192 discrete depths in 36 boreholes. The data were sampled from 1999 to 2006. Plotting of the depth-discrete CT data by 10-m depth intervals shows there is significant CT at depth, especially east of the known source area. A secondary data set also was used that supplemented the depth-discrete data taken while drilling with 88 measurements taken in completed wells using packers placed along the screened intervals to attempt to isolate discrete vertical zones of the unconfined aquifer. The average concentration of the packer data set (1,601 µg/L) was approximately four times higher than that of the depth-discrete data set (403 µg/L).

A minor issue that arose in review was the treatment of non-detect values in the current study. For the previous CT inventory estimation study documented in the letter report issued in January 2006, non-detect values were set to zero. For the current study, non-detects in the depth-discrete data set were not changed; non-detects in the packer data set were set to one-half the non-detect value. An evaluation of the effect of changing the non-detect treatment on the mean CT value found that the mean CT value of the depth-discrete data set would decrease from 382.6269 µg/L to only 382.3186 µg/L, a relative difference of only 0.0008. Given the strong dependence of the inventory values on the mean CT concentration, this indicates that the change would have minimal impact on the estimated inventory results, so with concurrence from FH (V. J. Rohay, personal communication, April 19, 2007), the decision was made not to revise the study to account for the preferred treatment of non-detect values.

The depth-discrete CT data were insufficient for defining a reliable 3D variogram model, so a horizontal variogram was calculated and modeled using a normal score transform of the FY05 CT data from the top of the aquifer. These data also were used as supplementary data for the geostatistical mapping of both data sets. The range of the vertical variogram model was assumed to be 30 m, based on analysis of the thickness of the plume using borehole data.

We used sequential Gaussian simulation to generate 1000 simulations of the CT and CF concentrations for the two data sets. Each simulation honors the available data, the variogram model, and the histogram of the concentration data. We used Tecplot to create a series of 3D visualizations of the median simulated CT and CF value at each node of the simulation grid, as well as the probability that the CT and CF concentrations exceed several concentration thresholds. Analysis of those visualizations suggests that the lower boundary of the plume is not well defined by the simulation grid, with high median concentrations of CT (>100 µg/L) present at the base of the simulation grid, which is located 60 m below the top of the unconfined aquifer.

The inventory of CT and CF was estimated within the geostatistical simulation grid using a Monte Carlo approach. The inventory reflects CT and CF present in the groundwater and sorbed to the sediment, with the CF assumed to represent CT that degraded early. The inventory simulations were based solely on aqueous concentration data from the two data sets, and no DNAPL is included in the inventory estimates. The Monte Carlo approach used to estimate the inventory attempted to account for uncertainty in the porosity and the K_d values for CT and CF by drawing values for those parameters from probability distributions.

A suite of 1000 values of the estimated CT inventory in the unconfined aquifer was generated from the 1000 simulations of CT and CF concentrations using the depth-discrete data sampled while drilling. The average value of the CT inventory based on CT and CF present in the aquifer for that data set is approximately 101,400 kg, and the 95% probability interval extends from 64,100 kg to 164,800 kg. The CT inventory appeared to be evenly split between the groundwater and the sediment, with a smaller amount present as CF. The CT inventory was also calculated for several concentration contours, with the highest proportion of CT associated with the 100–1000-µg/L contour interval. We also estimated the effect of hydrolysis on the CT that entered the aquifer and calculated an average value of approximately 132,000 kg of CT that would have originally dissolved in the aquifer to account for the 101,400 kg of CT and CF that was estimated to currently reside in the aquifer.

Simulation and inventory calculations performed using the combined data set that included packer data as well as the depth-discrete data suggested inventories of CT and CF distributed in the aquifer that were 7.4% higher, with a mean inventory of about 108,900 kg and a 95% probability interval derived from the simulations of 70,300 kg to 171,700 kg. Although a standard t-test suggests that the average inventory for the combined data set is significantly higher, there is wide uncertainty in the inventory simulations, with only a slight upward shift in the distribution of simulated inventory values.

Comparison of the inventory broken out by concentration levels for the combined data with those generated using just the depth-discrete data indicates that the majority of the difference between the two sets of inventory simulations occurs due to a decrease in the proportion of the simulated inventory occurring in the 100–1000-µg/L concentration interval and an increase in the proportion of the inventory occurring in the 2000–4000-µg/L concentration interval for the combined data set.

Analysis of the potential effect of hydrolysis on CT present in the aquifer for the two data sets suggests that between 132,000 and 143,500 kg of CT would have had to reach the aquifer to result in the current distribution of CT and CF. This would account for about 18% to 19% of the 750,000 kg of CT thought to have been originally disposed of in the 200 West Area, which is almost an order of magnitude higher than previous estimates of the disposed CT accounted for by the inventory in the unconfined aquifer (e.g., Rohay et al. 1994; Swanson et al. 1999).

Note that the estimated inventories derived for this study do not account for all CT known to be present in the area and therefore should be considered minimum values. One factor that would contribute additional inventory is the CT removed by the operation of the interim remedial actions that have occurred in the 200 West Area, including both soil gas vapor stripping and the operation of the groundwater pump-and-treat system. A second and more significant factor that indicates that the inventories are minimum values is the fact that the median concentrations exceed 100 µg/L over a fairly large area at the base of the simulation grid, which is 60 m below the top of the aquifer. This indicates that the lower limits of the plume are not well defined by the simulations, which are constrained by the extreme sparsity of data at depths that are greater than 60 m below the top of the aquifer. At least two wells, 299-W15-46 and 299-W13-1, have data with high concentrations below that depth, with the deepest data point from well 299-W13-1 having a CT concentration of 132 µg/L at a depth of 72.5 m. Both the data and the simulation results suggest that there is additional inventory present at depths greater than 60 m; additional data at those greater depths would be needed to estimate that inventory.

In conclusion, the geostatistical simulations of CT and CF concentrations prepared for this study, and the Monte Carlo estimates of CT inventory that were based on them, appear to provide a useful revision of earlier CT inventory estimates (e.g., Rohay et al. 1994; Swanson et al. 1999). The geostatistical inventory estimates presented here incorporate new information from more recently acquired depth-discrete data and packer data. The current version of the study documented here also includes a large quantity of additional depth-discrete data relative to the previous estimates documented in the letter report issued to FH in January 2006 (192 samples from 36 wells for the current study versus 141 samples from 26 wells for the study released in January 2006). These additional data reduced the uncertainty in areas where data from new wells were available, and additional improvements in the inventory estimates can be expected as new data become available in the future. The use of the packer data also added a substantial body of information to the inventory study. Additional work using the packer method would be useful in the future to allow estimates of the changing inventory with time. However, a much larger number of wells would need to be sampled over a wider area (e.g., covering at least the geographic area covered by the depth-discrete data) in order to cover the entire area of interest and provide reliable information on the change over time.

References

Cantrell KJ, RJ Serne, and GV Last. 2003. *Hanford Contaminant Distribution Coefficient Database and Users Guide* . PNNL-13895 Rev. 1, Pacific Northwest National Laboratory, Richland, WA.

Deutsch CV and AG Journel. 1998. *GSLIB: Geostatistical Software Library and User's Guide*. Oxford University Press, New York.

Goovaerts P. 1997. *Geostatistics for Natural Resources Evaluation*. Oxford University Press, New York.

Hartman MJ, LF Morasch, and WD Webber (eds). 2006. *Hanford Site Groundwater Monitoring for Fiscal Year 2005.* PNNL-15670, Pacific Northwest National Laboratory, Richland, WA.

Journel AG and M Rossi. 1989. When do we need a trend model in kriging? *Mathematical Geology* 21:715–739.

Murray CJ, Y Chien, and PD Thorne. 2004. *A Geostatistical Analysis of Historical Field Data on Tritium, Technetium-99, Iodine-129, and Uranium*. PNNL-14618, Rev. 0, Pacific Northwest National Laboratory, Richland, WA.

Oostrom M, ML Rockhold, PD Thorne, GV Last, and MJ Truex. 2004. *Three-Dimensional Modeling of DNAPL in the Subsurface of the 216-Z-9 Trench at the Hanford Site*. PNNL-14895, Pacific Northwest National Laboratory, Richland, WA.

Oostrom M, ML Rockhold, PD Thorne, GV Last, and MJ Truex. 2006. *Carbon Tetrachloride Flow and Transport in the Subsurface of the 216-Z-18 Crib and 216-Z-1A Tile Field at the Hanford Site: Multifluid Flow Simulations and Conceptual Model Update.* PNNL-16198, Pacific Northwest National Laboratory, Richland, WA.

Oostrom M, TW Wietsma, MA Covert, and VR Vermeul. 2007. Zero-Valent Iron Emplacement in Permeable Porous Media Using Polymer Additions. *Ground Water Monitoring and Remediation* 27(1):122–130.

Riley RG, DS Sklarew, CF Brown, PM Gent, JE Szecsody, AV Mitroshkov, and CJ Thompson. 2005. *Carbon Tetrachloride and Chloroform Partition Coefficients Derived from Aqueous Desorption of Contaminated Hanford Sediments*. PNNL-15239, Pacific Northwest National Laboratory, Richland, WA.

Rohay VJ, KJ Swett, and GV Last. 1994. *1994 Conceptual Model of the Carbon Tetrachloride Contamination in the 200 West Area at the Hanford Site.* WHC-SD-EN-TI248, Rev. 0, Westinghouse Hanford Company, Richland, WA.

Swanson LC, VJ Rohay, and JM Faurote. 1999. *Hydrogeologic Conceptual Model for the Carbon Tetrachloride and Uranium/Technetium Plumes in the 200 West Area: 1994 Through 1999 Update.* BHI-01311, Bechtel Hanford, Inc., Richland, WA.

Szecsody JE, JS Fruchter, JL Phillips, ML Rockhold, VR Vermeul, MD Williams, BJ Devary, and Y Liu. 2005. *Effect of Geochemical and Physical Heterogeneity on the Hanford 100D Area In Situ Redox Manipulation Barrier Longevity.* PNNL-15499 Rev. 1, Pacific Northwest National Laboratory, Richland, WA.

Thorne PD, ED Freeman, CR Cole, and EJ Freeman. 2001. Appendix D – Groundwater Data for Initial Assessment Performed with the System Assessment Capability (Revision 0). Web page referenced at http://www.hanford.gov/cp/gpp/modeling/sacarchive.cfm on 12/30/05.

Thorne PD, MP Bergeron, MD Williams, and VL Freedman. 2006. *Groundwater Data Package for Hanford Assessments.* PNNL-14753 Rev. 1, Pacific Northwest National Laboratory, Richland, WA.

Truex MJ, CJ Murray, CR Cole, RJ Cameron, MD Johnson, RS Skeen, and CD Johnson. 2001. *Assessment of Carbon Tetrachloride Groundwater Transport in Support of the Hanford Carbon Tetrachloride Innovative Technology Demonstration Program.* PNNL-13560, Pacific Northwest National Laboratory, Richland, WA.

Williams BA, FA Spane, VJ Rohay, and DB Erb. 2005. "Characterization of the Vertical Distribution of Carbon Tetrachloride Contamination in Hanford Site Groundwater." PNNL-SA-43094, presented to the Washington State 5th Annual Hydrogeology Symposium, April 12, 2005, Tacoma, WA.

This page intentionally left blank

Appendix – Carbon Tetrachloride Inventory Estimation and Uncertainty Quantification Approach

1. Loop over 1000 simulations
    a. Generate grid of values of CT concentration (ug/L) in GW by geostatistical simulation
    b. Generate grid of values of CF concentration (ug/L) in GW by geostatistical simulation
        i. Each simulation of CF generated independently, with no dependence on CT
    c. Draw value for Kd for CT for each simulation
        i. Triangular probability distribution with minimum of 0.106 L/kg and maximum of 0.367 L/kg (Riley et al. 2005), and most probable of 0.237 L/kg (average of min and max).
    d. Draw value for Kd for CF for each simulation
        i. Triangular probability distribution with minimum of 0.084 L/kg and max of 0.432 L/kg (Riley et al. 2005), most probable of 0.258 L/kg (average of min and max).
    e. For each grid cell in a simulation
        i. Draw value for total porosity from normal distribution with mean of 0.13 and SD of 0.033
            1. Porosity distribution for Ringold is same as that used for History Matching studies (Murray et al. 2004)
            2. Porosity and cell dimension provides volume of groundwater in each cell of simulation (L)
            3. Porosity, cell dimension, and assumed matrix particle density of 2.65 g/cc provides estimate of mass of sediment (kg) in each cell
                a. matrix particle density from Thorne et al. (2001)
                b. simulate fine sediment mass in cell for use in CT mass calculations based on Kd (corrected sediment mass).
                    i. If we assume that the gravel+ fraction has a porosity of 0.3 (Domenico and Schwartz 1990), then the porosity of the fines will be calculated using a stochastic total porosity with a mean of 0.13 and SD of 0.033 (Murray et al. 2004):
                        1. Porosity of fines = Stochastic value of total porosity / 0.3
                    ii. Mass of fines for Kd calculations can be estimated in each cell as
                        1. [cell volume * 0.3* particle density * (1- porosity of fines)].
        ii. Estimate mass of CT in groundwater
            1. Multiply groundwater concentration of CT (ug/L) by constant volume of groundwater in cell (L)
        iii. Estimate mass of CF in groundwater
            1. Multiply groundwater concentration of CF (ug/L) by constant volume of groundwater in cell (L)

iv. Estimate mass of sorbed CT in each grid cell using simulated value of CT and randomly drawn value of Kd for CT
    1. Multiply groundwater concentration of CT (ug/L) by Kd (L/kg) to get sediment concentration in ug/kg
    2. Multiply soil concentration (ug/kg) by corrected (fine) sediment mass (kg) to estimate mass of sorbed CT for that cell (ug)

v. Estimate mass of sorbed CF in each grid cell using simulated value of CF and randomly drawn value of Kd for CF
    1. Multiply groundwater concentration of CF by Kd to get soil concentration in ug/kg
    2. Multiply soil concentration (ug/kg) by corrected (fine) sediment mass (kg) to estimate mass of sorbed CF (ug) for that cell

vi. Convert mass of CF in cell to CT assuming CF generated by single-step reductive dechlorination of CT
    1. Add mass of CF in groundwater and sorbed to sediment to get total CF in cell
    2. Multiply CF mass (ug) by conversion factor to estimate mass of CT that degraded to CF
        a. Use molecular weight ratio of CT/CF = 154/118.5 = 1.3

vii. Add mass of CT in groundwater, mass of CT in sediment, and mass of CT estimated from CF to get total mass of CT in cell

viii. Add total mass of CT in cell to running totals for simulation
    1. Track total CT inventory as CT and due to CF separately
    2. Track grand total of CT inventory for each simulation
    3. Track totals partitioned by CT contour interval based on CT concentration in groundwater for each cell
        a. 5-100 ug/L
        b. 100-1,000 ug/L
        c. 1,000-2,000 ug/L
        d. 2,000-4,000 ug/L
        e. > 4,000 ug/L

2. Estimate effect of hydrolysis on original mass of CT that entered the aquifer
    a. Disposal occurred from 1955 to 1973 (Truex et al. 2001)
    b. Transport time through the vadose zone assumed to be 9 years (Oostrom et al. 2004), so CT entered aquifer from 1964 to 1982
        i. Assume average input date to aquifer of 1973
        ii. Assume representative date of depth-discrete CT data of 2004
        iii. Hydrolysis assumed to start approximately 31 years or 11,315 days ago.
        iv. Assume that degradation to CF happened by 1973, so only CT still present in aquifer as CT would be subject to breakdown by hydrolysis
    c. Abiotic breakdown rate (Ka) was estimated by Truex et al. (2001) to have a triangular probability distribution

i. minimum rate of breakdown of CT per day of 6.50E-06, a maximum rate equal to 5.30E-05, and a most probable rate of 1.90E-05.

ii. Draw 1,000 values of Ka from triangular probability distribution with parameters given above.

d. Estimated original mass of CT estimated original CT mass = current CT mass in aquifer and sediment (from viii.1, above) * (1/(1-Ka))**11,315 + CT inventory now associated with CF

References

Domenico PA and FW Schwartz. 1990. *Physical and Chemical Hydrogeology*. John Wiley & Sons, Inc., New York.

Murray CJ, Y Chien, and PD Thorne. 2004. *A Geostatistical Analysis of Historical Field Data on Tritium, Technetium-99, Iodine-129, and Uranium*. PNNL-14618, Rev. 0, Pacific Northwest National Laboratory, Richland, WA.

Oostrom M, ML Rockhold, PD Thorne, GV Last, and MJ Truex. 2004. *Three-Dimensional Modeling of DNAPL in the Subsurface of the 216-Z-9 Trench at the Hanford Site* . PNNL-14895, Pacific Northwest National Laboratory, Richland, WA.

Riley RG, DS Sklarew, CF Brown, PM Gent, JE Szecsody, AV Mitroshkov, and CJ Thompson. 2005. *Carbon Tetrachloride and Chloroform Partition Coefficients Derived from Aqueous Desorption of Contaminated Hanford Sediments*. PNNL-15239, Pacific Northwest National Laboratory, Richland, WA.

Thorne PD, ED Freeman, CR Cole, and EJ Freeman. 2001. Appendix D - Groundwater Data for Initial Assessment Performed with the System Assessment Capability (Revision 0). Web page referenced at http://www.hanford.gov/cp/gpp/modeling/sacarchive.cfm on 12/30/05.